[redacted]

[redacted]

ACR No. 3H30

C18Q1

NACA-WR-W 107

NATIONAL ADVISORY COMMITTEE FOR AERONAUTICS

MAY 15 1990

WARTIME REPORT

ORIGINALLY ISSUED

August 1943 as
Advance Confidential Report 3H30

INVESTIGATIONS ON LAMINAR BOUNDARY-LAYER STABILITY AND TRANSITION ON CURVED BOUNDARIES

By Hans W. Liepmann
California Institute of Technology

[redacted]

NOT REPRODUCIBLE

NACA

WASHINGTON

NACA WARTIME REPORTS are reprints of papers originally issued to provide rapid distribution of advance research results to an authorized group requiring them for the war effort. They were previously held under a security status but are now unclassified. Some of these reports were not technically edited. All have been reproduced without change in order to expedite general distribution.

W-107

Reproduced by
NATIONAL TECHNICAL
INFORMATION SERVICE
Springfield, Va. 22151

65

NATIONAL ADVISORY COMMITTEE FOR AERONAUTICS

ADVANCE CONFIDENTIAL REPORT

INVESTIGATIONS ON LAMINAR BOUNDARY-LAYER STABILITY AND TRANSITION ON CURVED BOUNDARIES

By Hans W. Liepmann

SUMMARY

Transition of the boundary layer from the laminar to the turbulent regime has been investigated on a flat plate, on the concave and convex side of a plate having a 20-foot radius of curvature, and on the convex side of a plate with a 30-inch radius of curvature. The investigations were carried out at the Guggenheim Aeronautics Laboratory, California Institute of Technology (GALCIT) in a special tunnel with low free-stream turbulence. It was found that transition was not affected by convex curvature in the investigated range from $\frac{\delta}{r} = 0$ to $\frac{\delta}{r} \doteq 0.001$. Concave curvature was found to have a pronounced effect on the transition point, decreasing the critical Reynolds number.

The laminar boundary-layer oscillations discovered recently by Fryden, Schubauer, and Skramstad on a flat plate have been investigated on the convex sides of the r = 20-foot and r = 30-inch plates. It was found that the mechanism of transition on the convex sides of the plates is the same as that on the flat plate. Measurements of the characteristics of the laminar oscillations agree closely with the results of Schubauer and Skramstad. The mechanism of transition on concave surfaces appears to be different from that for flat and convex plates.

Measurements of the influence of a single roughness element on the boundary layer show that transition can occur in two distinctly different ways downstream from the element: Transition can occur in the wake proper of the element or further downstream after the boundary layer has reattached itself to the surface.

The influence of a pressure gradient on transition on

NOT REPRODUCIBLE

the convex side of the r = 20-foot plate was studied. No definite parameter governing the influence of the pressure gradient has yet been obtained.

I. INTRODUCTION

The California Institute investigation of the effect of curvature on boundary-layer transition was initiated in 1937 under a general research program sponsored by the National Advisory Committee for Aeronautics. The purpose of this general program was to isolate the factors influencing transition - such as external turbulence, pressure gradient, and curvature - and to investigate each effect separately. The GALCIT undertook the investigation of the effect of curvature on the transition of the boundary layer from the laminar to the turbulent state.

The general nature of the problem requires the extreme reduction of all other factors influencing transition. Hence, the pressure gradient along the boundary should be as close to zero as possible and the external turbulence level as low as possible. To satisfy the first condition, the curved surface was chosen as a thin sheet set into a curved test section such that the test sheet and the walls of the section form four concentric cylinder surfaces. To reduce the turbulence level of the free stream the flow upstream of the test section had to be carefully controlled. These two conditions determine essentially the type of wind-tunnel equipment used in this investigation, which is described in a later part of this report. The flat plate at zero pressure gradient is the limiting case for large radius of curvature, and thus forms the link between this investigation and the research on the influence of turbulence level and laminar boundary-layer oscillations on transition carried out on a flat plate at the National Bureau of Standards in the course of the same general program of the NACA.

The first investigations on the influence of curvature on transition by Milton and Francis Clauser (reference 1) at GALCIT showed a strong influence of curvature on the location of the transition point. Convex curvature was found to delay transition appreciably as compared with concave curvature. These results, however, met with some criticism based mainly on the following two points: In the experiments of the Clausers the angle of attack of

the curved sheet was not varied. Hence, the concave side and the convex side of the sheet, respectively, were tested under flow conditions not necessarily identical, since the stagnation point might have been situated on the convex or the concave side. Since Schiller (reference 2) and Hall and Hislop (reference 3) found a strong angle-of-attack effect in their research on flat plates, it was suggested by Taylor (reference 4) that the curvature effect of the Clausers could have been influenced by the initial setting of the plate.

This criticism was aggravated by the fact that in the investigation of the Clausers, only concave and convex curvature had been investigated, but no measurements of the transition on a flat plate had been carried out.

The unpublished research conducted by A. C. Charters, Jr., of C.I.T. during 1938-39 was mainly undertaken to check the validity of this criticism. A detailed discussion of the main results of investigations by the Clausers and Charters is given in a later part of this report. The general result of Charters' investigation was that the angle-of-attack effect did not account for the results found by the Clausers. Attempts to close the other gap in the Clausers' experiments, namely, the investigation of flat-plate flow under the same conditions as the flow past the curved sheet, met with considerable difficulty which forced a postponement of the further investigation of curvature effect in order to allow for a separate investigation of flat-plate flow (reference 5).

A new attempt to determine the effect of curvature was started in 1940. The present report presents the results of this research.

The theoretical aspect of the influence of curvature on transition is closely interwoven with the theoretical aspect of the whole transition problem. Transition must be brought about by some instability of the laminar flow. Investigations of the stability of laminar flow with respect to small perturbations of various forms have been carried out by a number of investigators. It appears that there exist two distinctly different types of instability of laminar motion which may be termed (1) "dynamic," and (2) "viscous" instability:

(1) We call a motion dynamically unstable if, under neglect of the viscous forces, small perturba-

NOT REPRODUCIBLE

tions of the mean velocity profile increase with time. To be sure, this includes flows which can only exist in viscous fluids; as a matter of fact, in most cases viscosity is necessary to produce the mean velocity profiles involved. Such dynamic instability has been found, for example, in the case of profiles with inflection points (references 6 and 7) and in certain problems of curved flow (references 8, 9, and 10). In general, if the viscosity is taken into account in such cases the influence of viscosity narrows the range of Reynolds number in which instability occurs. In other words, the viscosity has the effect of decreasing the instability of such flows.

(2) There are, however, cases where the influence of friction on the perturbation is just the opposite. The viscous forces here are essential to bring about an energy transfer from the mean motion into the perturbation motion. If the viscosity is neglected, the flow is found to be perfectly stable. The most important case of stability of the boundary layer of a flat plate belongs in this class (references 11 and 12). The Blasius layer was found by Tollmien (reference 11) to be subject to this type of viscous instability.

The results of such investigations of viscous instability, which were mainly advanced by the Göttingen group, did not, however, meet with universal acceptance. The reason for this is found in the lack of experimental evidence - especially in the case of the flow along a flat plate - and also in the mathematical and physical not-quite-convincing assumptions and methods of approximation used in these theories.

On the other hand, the results of the theoretical investigations revealing dynamic instabilities have been generally accepted. Theories of boundary-layer transition, based on the assumption that finite external influences such as turbulence or an adverse pressure gradient change the mean velocity profile to a dynamically unstable form, were therefore proposed. This point of view was especially advanced by G. I. Taylor (reference 4).

The influence of curvature on boundary-layer transition belongs essentially in the class of dynamic instability.

As a matter of fact, it was predicted that the centrifugal and Coriolis forces should produce stability and instability ranges of the same general character as are observed in the case of rotating cylinders (reference 8).

The recent discovery of the sinusoidal boundary-layer oscillations by Schubauer and Skramstad (reference 14) at the National Bureau of Standards and the investigation of the behavior of these oscillations gave the first clear experimental confirmation of the Tollmien and Schlichting theories of viscous instability. This experimental result decisively influenced the approach of the entire transition problem. Owing to the exchange of progress reports - through the NACA - between the N.B.S. and the GALCIT, the author was fortunate in having advance knowledge of these investigations, and the research program was strongly influenced by this most important interchange.

The results presented in this report show that the character of boundary-layer transition at a convex boundary is the same as on the flat plate. The parameters of the laminar boundary-layer oscillations agree with the results of Schubauer and Skramstad on the flat plate. A slight stabilizing effect of convex curvature is barely noticeable in the investigated range and is of no practical importance. Concave curvature, however, was found to have a strong destabilizing effect, in agreement with theoretical expectation, regarding a dynamic instability due to centrifugal forces. The present investigation gives a general survey of this "concave" case, although the results are not quite so complete as in the case of the flat plate and convex walls.

This investigation, conducted at the California Institute of Technology, was sponsored by, and conducted with financial assistance from, the National Advisory Committee for Aeronautics. Dr. Th. von Kármán and Dr. C. B. Millikan supervised the research. The author wishes to express his sincere appreciation and thanks for their encouragement and advice.

Mr. Carl L. Thiele and Mr. Stanley Corrsion's cooperation and Mr. Phillip Johnson's assistance during various parts of the investigation are gratefully acknowledged.

NOT REPRODUCIBLE

II. SYMBOLS

x, y, z	orthogonal coordinates { The boundary surface is represented by $y = 0$. The X axis points from the leading edge in the direction of the main flow }
r	radius of curvature of the boundary surface
u, v, w	local mean velocity
U	mean velocity of the free stream
u', v', w'	components of the velocity fluctuations in x, y, and z direction
$\frac{u'}{u} = \sqrt{\frac{\overline{u'^2}}{u^2}}$, etc.	root mean square of the relative velocity fluctuation
ρ	density
ν	kinematic viscosity
$\eta = y\sqrt{\frac{U}{\nu x}}$	Blasius' nondimensional parameter
δ	boundary-layer thickness
ϑ	momentum thickness of the boundary layer
δ^*	displacement thickness of the boundary layer
R	Reynolds number
R_x, R_ϑ, R_{δ^*}	Reynolds number based on x, ϑ, and δ^*, respectively
$R_{x_{tr}}$, $R_{\vartheta_{tr}}$, $R_{\delta^*_{tr}}$	Reynolds number of the transition point
$\beta_r = 2\pi$ times the frequency f	of the Tollmien-Schlichting waves
$\alpha = 2\pi$ divided by the wave length λ	of the Tollmien-Schlichting waves
c_r phase velocity	of the Tollmien-Schlichting waves
β_i amplification factor	of the Tollmien-Schlichting waves
$\alpha = 2\pi$ divided by the wave length	of the Taylor-Görtler vortices
β amplification factor	of the Taylor-Görtler vortices
r=20-foot plate, r=30-inch plate	= plates having 20-foot and 30-inch radius of curvature, respectively

III. APPARATUS AND METHODS

1. The Wind Tunnel

Figure 1 shows the wind tunnel especially built for for this research. The somewhat unconventional design is due to the following requirements:

(a) The tunnel should possess test sections of various curvatures which are easily interchangeable

(b) The test sections must have a large aspect ratio (8:1) in order to prevent secondary flow in the curved sections

Because of these reasons a pressure-type tunnel was chosen by the Clausers (reference 1), and the general layout of the present tunnel resembles very much that described by them. The pressure in the test section of a tunnel of the type shown in figure 1 can be adjusted by means of flaps and screens at the diffuser exit. Thus the test section can be operated without large pressure differences acting on the walls. This is an essential point for the construction of high and narrow test sections as employed in this investigation.

The tunnel is operated by a 68-horsepower stationary natural-gas engine which drives two 8-blade fans. The speed is remotely controlled by means of a small electric motor which drives the throttle through a gear and lead-screw system. This gas engine was chosen as a result of financial and electric power considerations, and has proved very satisfactory. The velocity range of the tunnel is about 5 to 40 meters per second.

2. Turbulence Level

The turbulence level in the test section of the tunnel is controlled by two screens and one honeycomb followed by a 10:1 contraction (fig. 1). The screens are seamless precision screens; 18 mesh per inch, wire diameter 0.018 inch. The honeycomb consists of some 6000 paper mailing tubes, 6 inches long and 1 inch in diameter. The main turbulence-controlling device is actually the screen farthest downstream. The honeycomb and first screen serve mainly to smooth the very irregular flow entering the settling chamber.

The turbulence in the test section was found to be

$$\frac{u'}{u} = 0.06 \text{ percent}$$

$$\frac{v'}{u} = \frac{w'}{u} = 0.12 \text{ percent}$$

At the highest obtainable speeds the value of u'/u was found to increase to about 0.09 percent. Correlation measurements showed that the correlation function for the tunnel turbulence did not resemble an exponential function as in the case of isotropic turbulence. The correlation coefficient $\frac{\overline{u_1' \quad u_2'}}{\sqrt{\overline{u_1'^2}} \quad \sqrt{\overline{u_2'^2}}}$ was found to drop over a distance of about 1/4 inch from 1 to about 0.7 but from then on decreased very slowly over a distance of 2 inches to about 0.5.

This shows that the turbulence in the free stream is quite different from isotropic turbulence. This in agreement with the results of Schubauer and Skramstad (reference 14), which showed that a large part of the tunnel turbulence at low levels consists of sound. The "scale" of this pseudoturbulence is evidently very large.

3. The Test Sections

The tunnel possesses three interchangeable test sections of different curvature: $r = \infty$, $r = 20$ feet, $r = 30$ inches. The height of the sections is 5 feet; the length, 7 feet; the width, 7.5 inches. The construction is essentially the same for the three sections. They consist mainly of three plate-glass plates of 1/4-inch thickness. Two of these plates form the walls of the section; the third plate, set in the middle of the section, forms the test sheet. In the case of the curved sections, the radius of curvature given is the one of the test plate; the walls form concentric cylinders. The leading edges of the test plates are ground and polished over about a 2½-inch length to a leading edge of 1/32-inch radius of curvature.

The side plates of these sections can be moved out and in at both the trailing and leading edges and the test plate can be rotated about a pivot situated in line with the lead-

ing edge. Pressure gradient and angle of attack can thus be adjusted within fairly wide limits.

4. Traversing Mechanism

Earlier investigations have shown that for a complete investigation of the boundary layer and of transition, a continuous traverse with the measuring instrument along the plate (in x-direction) and normal to the plate (in y-direction) is very essential. The narrow test sections, which leave on both sides of the test plates channels only $3\frac{3}{4}$ inches wide and, in addition, the curvature of the sections, made a continuous traverse difficult. The construction of the traversing mechanism is therefore presented in some detail:

Figure 2 shows the general scheme of the arrangement drawn for the section with the largest curvature (r = 30 inches). The actual track mechanism, which has to be rather heavily built, is removed from the test section into the diffuser. A frame formed of heavy streamline steel tubing slides in tracks running along the top and bottom of the diffuser. This unit is propelled by means of a chain and sprocket driven by a reversible-speed direct-current motor by remote control. The measuring instruments - hot wires, static tubes, and so forth - are mounted on small carriages of the type shown in figure 3. These carriages are guided along the plate by long arms extending from the steel frame in the diffuser into the test section. These arms are made of dural tubing in partitions connected by brass hinges to allow the carriage to follow the curved plate. The number of partitions was four for the r = 30-inch plate, two for the r = 20-foot plate, and one for the flat plate.

The carriages are held on the test plate by means of a spring-loaded lever pressing against the wall of the section. This arrangement made possible a continuous traverse in the x-direction of about 6 feet. To traverse across the boundary layer in the y-direction, the instrument on the carriage can be tilted by means of a micrometer screw which, in turn, is operated by means of a flexible shaft running alongside the arm (fig. 2) to a small reversible-speed electric motor mounted on the track in the diffuser. Thus, a continuous traverse of about $2\frac{1}{2}$ inches normal to the plate is accomplished.

The x and y positions are read through the glass wall on a paper scale giving the distance from the leading edge, and on the calibrated micrometer screw on the carriage, respectively.

In the z-direction the arm can be set discontinuously by moving the clamps which fasten the arm to the steel frame in the diffuser. Figure 4 shows the r = 20-foot section with the traversing arm in the forward position.

This type of traversing mechanism worked very satisfactorily, both for the concave and the convex side of the plates. Since the main unit is mounted in the diffuser, only the arms have to be replaced when changing to another test section.

5. Hot-Wire Apparatus

Hot wires have been extensively used in this investigation. All velocity profiles and, of course, all measurements of fluctuations were made with the hot-wire anemometer. The determination of the transition point was, in earlier measurements, made by means of the surface-tube technique, but in later measurements a hot wire was employed.

The hot-wire equipment can be split up into the hot-wire anemometer proper, the electrical apparatus for mean-speed measurements and, finally, the apparatus used for the study of velocity fluctuations.

(a) Hot-wire anemometer.- The hot wires used consisted of platinum wire 0.0005 inch and 0.00024 inch thick for mean-speed and velocity-fluctuation measurements, respectively. The platinum wire was always soft-soldered to the tips of fine sewing needles. The silver cover of the 0.00024-inch wire (Wollaston wire) was removed before soldering the wire to the needles. The hot-wire holders consisted of ceramic tubing (so-called Stupakoff tubing) about 5 inches long. This tubing is available with either two or four holes - the diameter being about 0.14-inch and 0.3-inch, respectively. The needles were soldered to copper wires which were cemented into the holes of the ceramic tubing. A holder of this type is seen in figure 3.

The wires used for measuring mean speed were generally about 3 millimeters long; velocity fluctuations par-

allel to the mean flow (u') were measured with a single wire about 2 millimeters long; fluctuations normal to the mean flow (v', w') were measured with two 3-millimeter long wires, mounted in x form. The wires were mounted in two parallel planes as close together as possible. The angle between the wires was between 60° and 80°; the angle with the direction of the wind was therefore between 30° and 40°.

(b) Equipment for mean-speed measurements.- For measuring mean speed, both the constant-current and the constant-resistance methods were employed. These methods are described in the literature (for example, reference 15). Generally, the constant-resistance method was preferred, owing to the constant sensitivity of the wire throughout a velocity profile, which permitted operation of the wire at rather low temperature (about 40° C above air temperature). This lessens the errors introduced by convection currents and heat loss to solid boundaries. The measuring instruments consist mainly of a Wheatstone bridge for measuring the resistance of the wire, and a potentiometer for measuring the current through the wire or the voltage across the wire. This mean-speed apparatus is made up of two identical circuits which, with the necessary switching devices, allow the operation of two separate hot wires and the measurement of the sum or the difference of the voltages across the wires. The apparatus, together with the amplifier described in the next section, is built in one large steel cabinet to avoid external electrical disturbance.

The whole apparatus was designed and built by Carl Thiele.

(c) Apparatus for turbulence investigation.- The main part of this equipment consists of an alternating-current amplifier to amplify voltage fluctuations across the wires. The amplifier used had a frequency response uniform within about ±3 percent from about 5 to 9000 cycles per second. For the compensation of the time lag of the wire, an inductance circuit with variable compensation resistance is provided. The output of the amplifier is measured by means of a thermocouple and wall galvanometer. The whole unit is battery-operated to lessen the pickup from external disturbances. The time constants of the wires were determined by the electrical-oscillator method (reference 15). Large chokes in the heating circuits of the wires assure constant-current operation.

Auxiliary equipment includes oscilloscopes, sound analyzer, oscillator, an electronic switch to allow observation of two signals with one oscilloscope and, finally, a frameless General Radio motion-picture camera for photographing oscillograms.

6. Measurement of Pressure Distribution Angle of Attack

The pressure distribution along the plates was measured with a small static tube made from a hypodermic needle. The tube was mounted on the carriage at a distance of about 1 centimeter from the boundary, and the pressure along the plate was measured at this constant distance. It was soon found that the pressure along the plates was not uniform but showed irregular maximums and minimums. The setting of the walls improved the over-all gradient but did not remove the waviness of the distribution. Flexible walls on the top and the bottom were tried but showed little effect. It was then concluded that the "waves" in the distribution were due to local changes in radius of curvature of the test plate. This was confirmed by comparing the pressure distribution on both sides of the plate and by observation of the distance of a hot wire from the plate set very close to the boundary and moved along on the three-legged carriage. This variation in radius of curvature limits the accuracy with which the pressure gradient can be set to zero. As expected, this effect was largest for the sharply curved plate. It is believed, however, that the residual pressure gradients did not appreciably affect transition. The pressure distributions for zero gradient are shown in figure 5.

In all measurements on the curved plates, the angle of attack was set to a favorable value; that is, the stagnation point was put on the investigated side of the test plate. During the investigations of the flat plate, it was attempted to set the angle of attack to zero by measuring simultaneously on both sides of the plate. The setting of the stagnation point determines naturally the pressure distribution over the first few inches of the plate. A discussion of this effect in connection with the results obtained by the Clausers is given later on.

7. Determination of the Transition Point

Transition was determined in earlier measurements with the surface-tube technique. (See, for example, reference 5.) This technique uses essentially the difference in velocity close to a solid wall in a laminar and a turbulent layer to determine transition. Later, visual observation of velocity fluctuations measured by a hot wire on the screen of a cathode-ray oscilloscope was applied to determine transition. This method uses, essentially, the fact that the flow in the transition region alternates between a laminar (Blasius) and a turbulent (v. Kármán) profile. This causes large sudden velocity changes close to the plate - the so-called turbulent bursts. The first appearance of these bursts was taken as the transition criterion. The locations of the transition points determined in this manner agree satisfactorily with points measured with the surface-tube technique, where the minimum head (i.e., shear) is taken as transition criterion.

IV. INVESTIGATION OF THE FLOW ALONG A FLAT PLATE

Before any attempt to determine the effect of curvature on transition was made, the flow along a flat plate was investigated.

The purpose of this investigation was:

(a) To determine whether a stable laminar boundary layer with a clearly defined transition point could be obtained in a tunnel of the type shown in figure 1 (As mentioned before, it was found difficult to determine transition on a flat plate in the tunnel of the Clausers.)

(b) To determine the Reynolds number of transition at zero pressure gradient for this limiting case, $r=\infty$

(c) To develop the necessary technique for the investigation of the effect of curvature on transition

1. Mean speed distribution in the laminar boundary layer was measured with the hot-wire anemometer using the constant-resistance method. The result is shown in figure 6.

The agreement with the theoretical Blasius distribution is very good. The wires were operated at low temperature and the heat loss toward the glass plate is seen to be negligible, since even the points closest to the plate do not show any marked deviation toward higher velocities.

2. Transition Point

The transition point was determined by means of the surface-tube technique. The pressure gradient was set as close to zero as possible; figure 5 shows the actual pressure distribution along the plate. The angle of attack of the plate was set so that transition occurred at about the same distance from the leading edge on both sides of the plate. The measured Reynolds number of transition based on the distance from the leading edge was about 2×10^6. Measurements with a "stable" angle of attack - that is, turning the stagnation point on the investigated side gave a Reynolds number of about 2.5×10^6. The pressure gradient in this latter case, however, was slightly favorable and the increase in Reynolds number of transition is therefore possibly not due to angle-of-attack effect only.

These values are somewhat lower than Schubauer and Skramstad's results (reference 14) for the same turbulence level. For $\frac{100\sqrt{u'^2 + v'^2 + w'^2}}{\sqrt{3\,u^2}} = 0.11$ (the value of the free-stream turbulence of the present investigation) Schubauer and Skramstad give: $R_x \doteq 2.7 \times 10^6$. A possible explanation for this discrepancy is given in a later part of this report.

3. Velocity Fluctuations in the Boundary Layer

The velocity fluctuations, especially in the laminar boundary layer and in transition, were studied in some detail. All three components of the fluctuations have been measured. The results are shown in figures 7 and 8. The results of this investigation do not now seem to be of as great interest as was thought to be the case when these measurements were carried out. This is due to the discovery of the laminar boundary-layer oscillations which will be discussed in a later part of this report. Only the main conclusions, therefore, are given here:

It is seen from figures 7 and 8 that, in the laminar layer v' and w' - that is, the fluctuations normal to the mean flow - are of much smaller amplitude than is u'. With increasing Reynolds number, u', v', w' increase in the laminar layer, keeping about the same ratio of $u':w':v'$. In the fully developed turbulent layer, the values of

v', w', and u' are of the same order. The large fluctuations occurring in the transition region itself have to be considered separately, since the larger part of these fluctuations is due to a sudden change in mean speed rather than true random fluctuations about a mean value. Figure 9 illustrates the $\left(\frac{u'}{u}\right)$ velocity fluctuations which may be expected to occur in the transition region: The mean velocity distribution alternates between a laminar (Blasius) profile and a turbulent (v. Kármán) profile. The velocity close to the wall will therefore suddenly rise from $(u)_{laminar}$ to $(u)_{turbulent}$, drop again to $(u)_{laminar}$, and so on. The velocity close to the outer edge of the laminar layer does the same, but the phase is reversed since here (see fig. 9) the turbulent profile gives a smaller velocity than the laminar profile. This explains the two maximums found in the $\frac{u'}{u}$ distribution by some investigators (references 16 and 17). Figure 10 shows an oscillogram of these fluctuations observed near the wall. The one-sided character is clearly seen. These turbulent bursts are typical of transition and in later investigations transition was often determined by their appearance.

V. EFFECT OF CURVATURE ON THE TRANSITION POINT

The effect of curvature on the transition point is presented here, before a discussion of the laminar boundary-layer oscillations is given. This choice was made as a result of the belief that the basic conceptions of the influence of curvature on transition, which led to this investigation, should be outlined first and compared with the results of measurements of the transition point by conventional methods. The investigation of the laminar boundary-layer oscillations required a quite-different technique, and the scope of this second type of research is rather different from that originally planned.

1. Effect of Curvature on the Mean Flow in the Boundary Layer

The Navier-Stokes equations for two-dimensional motion are:

$$u \frac{\partial u}{\partial x} + v \frac{\partial u}{\partial y} = - \frac{1}{\rho} \frac{\partial p}{\partial x} + \nu \left(\frac{\partial^2 u}{\partial x^2} + \frac{\partial^2 u}{\partial y^2} \right) \tag{1a}$$

$$u \frac{\partial v}{\partial x} + v \frac{\partial v}{\partial y} = - \frac{1}{\rho} \frac{\partial p}{\partial y} + \nu \left\{ \frac{\partial^2 v}{\partial x^2} + \frac{\partial^2 v}{\partial y^2} \right\} \tag{1b}$$

The theory of boundary-layer flow assumes that the thickness δ of the layer in which the viscous and inertia terms are of the same order is small compared with the length l of the layer measured from the stagnation point. Thus,

$$\frac{\partial}{\partial x} \sim \frac{1}{l} << \frac{\partial}{\partial y} \sim \frac{1}{\delta}$$

and

$$\frac{v}{u} \sim \frac{\delta}{l}$$

Neglecting terms δ/l and higher, the boundary-layer equation results from (1a)

$$u \frac{\partial u}{\partial x} + v \frac{\partial u}{\partial y} = - \frac{1}{\rho} \frac{\partial p}{\partial x} + \nu \frac{\partial^2 u}{\partial y^2} \tag{2}$$

since the balance of viscous and inertia forces in the layer requires

$$\delta^2 \sim \nu$$

All velocity terms in (1b) are of the order δ/l or higher; hence it follows:

$$\frac{\partial p}{\partial y} \sim \frac{\delta}{l}$$

Consequently, the pressure gradient across the layer for plane motion is of the order δ/l, and therefore its influence on the mean speed distribution neglected. The experimental verification of the computed velocity profile in the case of the flat plate proves these assumptions to be justified.

If curvature of the surface is taken into account, it follows that the pressure across the boundary layer is no longer constant but that there must exist a pressure gradient to balance the centrifugal force. If x denotes the circumferential coordinate, y the normal distance from the curved surface, u and v the circumferential and radial velocity components, respectively, the boundary-

layer equation remains, in first approximation,* unaltered. But there appears a second equation, giving the balance between centrifugal forces and pressure gradient across the layer:

$$\frac{\rho u^2}{|r|} = \pm\frac{\partial p}{\partial y} \begin{cases} + & \text{for concave boundaries} \\ - & \text{for convex boundaries} \end{cases} \qquad (3)$$

Hence there now exists a difference of pressure in the boundary layer normal to the mean flow of the order

$$\frac{\Delta p}{\frac{1}{2}\rho u^2} \sim \frac{\delta}{r} \qquad (4)$$

This shows that the effect of curvature should depend on the parameter δ/r. Since δ is a function of the velocity U, the parameter can be changed at a given radius of curvature by varying the speed. This makes an investigation of the effect of curvature over a wide range of δ/r with a limited number of test plates possible. As a practical parameter, δ is not particularly suitable since δ is relatively indefinite; δ is therefore replaced by either δ^*, the displacement thickness of the boundary layer, or by ϑ, the momentum thickness of the layer.

The experimental check showed that the influence of curvature on the mean velocity profile was negligible throughout the investigated range - that is, up to $\frac{\delta}{r} = 0.001$. The velocity profiles, measured on the curved plates, agreed very well with the Blasius distribution for the flat plate. Hence, in all computations the velocity profile is taken as the Blasius profile. Momentum and displacement thickness were thus taken as:

$$\vartheta = \frac{2}{3}\sqrt{\frac{\nu x}{U}}$$

$$\delta^* = 1.73\sqrt{\frac{\nu x}{U}}$$

NOT REPRODUCIBLE

2. Effect of Curvature on Boundary-Layer Transition

The following consideration of the stability of curved boundary-layer flow is due to Rayleigh (reference 18) and

*r, the radius of curvature, is assumed to be large compared with δ.

Prandtl (reference 19). Consider a particle of fluid in the boundary layer having a velocity u_0. The equilibrium condition (equation (3)) gives:

$$\frac{\rho u_0^2}{|r|} = \pm \left(\frac{\partial p}{\partial y}\right)_0$$

If this particle is displaced from its original position in the y (or r) direction, it enters a layer in which the velocity is, say, u_1, and therefore

$$\frac{\rho u_1^2}{|r|} = \pm \left(\frac{\partial p}{\partial y}\right)_1$$

during this motion the particle has to conserve its angular momentum $u\,r$. For small δ/r, r can be assumed as constant throughout the layer. Hence, $u = u_0$. Consider first the concave side of the plate: If the particle is moved outward from the wall

$$\frac{\rho u_1^2}{|r|} > \frac{\rho u_0^2}{|r|}$$

Hence, the centrifugal force acting on the displaced particle is less than that acting on the surrounding fluid, and under the influence of the pressure gradient the particle tends to move further in the same direction. If the particle is displaced inward $\frac{\rho u_0^2}{|r|} > \frac{\rho u_1^2}{|r|}$ and the particle has again the tendency to continue in the same direction; that is, the flow appears to be unstable. On the convex side of the plate, the same considerations show that the flow should be stabilized. Based on this consideration, transition was expected to be delayed on the convex side of a curved sheet and precipitated on the concave side. It is interesting to note in this connection that the flat-plate boundary layer has to be considered slightly convex curved since the second-order pressure gradient across the layer is equivalent to a slight convex curvature.

$$\left(-\frac{1}{r}\right) \sim \frac{\partial}{\partial x}\frac{v}{u} \sim \frac{\partial}{\partial x}\frac{\delta}{x}$$

Now for the Blasius layer:

$$\delta \sim \sqrt{\frac{\nu x}{U}}$$

hence

$$\left(-\frac{1}{r}\right) < 0$$

$$\left|\frac{1}{r}\right| \sim \frac{1}{x}\frac{1}{\sqrt{R_x}} \tag{5}$$

$$\frac{\delta}{r} \sim \frac{1}{R_x} \tag{6}$$

The experimental results of transition measurements on the convex and concave sides of the $r = 20$-foot plate together with the results on the flat plate are presented in figure 11. The Reynolds number of transition $R_{\vartheta_{tr}}$, based on the momentum of thickness ϑ, is plotted as function of ϑ/r. Negative values of δ/r correspond to concave, positive values to convex curvature.

It is seen that the Reynolds number of transition on the convex side of the $r = 20$-foot plate does agree, within the experimental scatter, with the result found for the flat plate.

Concave curvature is seen to have a marked destabilizing effect on the boundary layer. The values for $R_{\vartheta_{tr}}$ found on the concave side of the $r = 20$-foot plate are considerably lower than the values for the flat plate and decrease with increasing $\frac{\vartheta}{r}$.

The transition point was then investigated on the convex side of the $r = 30$-inch plate at different free-stream velocities and thus at different values of ϑ/r. The values of ϑ/r which could be reached in this way extended from $\frac{\vartheta}{r} = 0.6 \times 10^{-3}$ to about 2.0×10^{-3} ; that is, they are about one order of magnitude larger than those obtainable with the 20-foot plate (fig. 11). The first measurements led to the surprising result that the Reynolds number of transition decreased from a value of $R_x = 2.2 \times 10^6$ at the smallest value of ϑ/r, to about 0.5×10^6 at the highest value of ϑ/r.

Although the highest transition Reynolds number thus found corresponded very well to the measurements on the flat plate and on the 20-foot plate, the sudden decrease

in Reynolds number was suspected of being caused by an influence other than the curvature. Since the lowest values of the critical number were measured at the lowest speed and thus at the greatest distance from the leading edge of the plate, an influence of the spreading of turbulence from the turbulent boundary layer on the outer (concave) wall inward toward the center plate was suspected as the factor causing the early transition at low speeds. Measurements of the turbulence level close to the edge of the laminar boundary layer of the center plate showed that this assumption was correct. Figure 12 gives the result of this survey. It is seen that the turbulence level u'/U is nearly constant and equal to the normal free-stream level of about 0.06 percent up to $x = 60$ centimeters. Farther downstream, the turbulence level increases rapidly to a value of 0.75 percent at $x = 135$ centimeters. This increase in turbulence level is certainly large enough to decrease the value of the critical number.

An attempt could be made to correct these transition measurements by using the results of the N.B.S. on the influence of the free-stream-turbulence level on the location of the transition point. Such a correction, however, is rather doubtful for the following reasons: The measurements at the N.B.S. were made with a turbulence level very nearly constant along the laminar boundary layer from the leading edge to the transition point. In the curved tunnel, the boundary layer is influenced by a turbulence level which is constant up to a certain distance from the leading edge and increases steadily thereafter. Furthermore, the spectrum of the turbulence will have a certain influence and it is therefore not certain if the N.B.S. results are directly applicable.

It is believed that the measurements up to about $\frac{\vartheta}{r} \doteq 0.001$ are not appreciably affected by this spread of turbulence. The combined results of the measurements on the flat plate, the 20-foot, and the 30-inch plate (up to $\frac{\vartheta}{r} = 10^{-3}$) are plotted in figure 13. Convex curvature has apparently no appreciable effect on the point of transition from the laminar to the turbulent state of the boundary layer.

The spread of turbulence from the boundary layer along the concave wall is interesting and worth an investigation, especially since this problem might occur in the design of closed return low-turbulence wind tunnels.

The influence of concave curvature is in agreement with the consideration of Rayleigh and Prandtl, discussed above. This result, together with the lack of any stabilizing effect of convex curvature, suggests that the mechanism of transition is the same for the flat plate and the convex curved surfaces, but different from the mechanism leading to transition on concave surfaces. That the boundary layer on the flat plate does not represent the exact limit between concave and convex curvature, but is to be considered as slightly convex, was pointed out above.

This consideration leads logically to a more detailed investigation of the mechanism of transition.

VI. BOUNDARY-LAYER STABILITY

1. Theoretical Discussion

The question as to the stability of a given laminar velocity distribution is one of the most important and, mathematically, most difficult problems in fluid mechanics. To treat the problem analytically, the following assumptions are generally made:

(1) The mean velocity u is parallel to x and is only a function of y

(2) The perturbation velocities u', v', and w' are considered so small that squares and higher-order terms of u'/u, and so forth, can be neglected

Since assumption (2) leads to linear differential equations, u', v', and w' can be chosen as simple functions (for example, harmonics) and the general perturbation can be built up as the sum of these simple functions. If the motion is found to be unstable - that is, if u', v', and w' increase with time, the theory can only be expected to hold for the initial state; that is, as long as u', v', and w' are so small that the linear approximation (2) is applicable. Hence, a theory based on the above assumption is able to predict the breakdown of laminar flow but not able to give the development of turbulent flow, since this involves a change in the basic profile and represents, therefore, a nonlinear phenomenon.

In connection with the curvature effect on transition, two types of perturbation fluctuations which have been theoretically investigated are of main interest:

(a) The two-dimensional perturbation given by the stream function

$$\psi(x,y,t) = \varphi(y)\, e^{i(\alpha x-\beta t)} \tag{8}$$

where α is taken as real, β as complex, $\beta = \beta_r + i\beta_i$

(b) The three-dimensional perturbation given by:

$$\begin{aligned} u' &= \gamma_1(y) \cos(\alpha z)\, e^{\beta t} \\ v' &= \gamma_2(y) \cos(\alpha z)\, e^{\beta t} \\ w' &= \gamma_3(y) \sin(\alpha z)\, e^{\beta t} \end{aligned} \tag{9}$$

where both α and β are real quantities.

(α) Using the assumptions (1) and (2) and the two-dimensional perturbation (8), the Navier-Stokes equation can be reduced to the so-called Sommerfeld equation:

$$(u-c)\,(\varphi''-\alpha^2\varphi) - u''\varphi = -\frac{i\nu}{\alpha}\,(\varphi^{IV} - 2\alpha^2\varphi'' + \alpha^4\varphi) \tag{10}$$

where the real part of $c = \frac{\beta}{\alpha}$ is the phase velocity of the "wave" (equation (8)). The determination of φ from equation (10) for a given $U(y)$ and given boundary conditions is only possible for certain values of α, c, and a characteristic Reynolds number of the problem. The sign of the imaginary part of these "eigenvalues" for c determines whether the perturbation is positively or negatively damped, since

$$\beta_r + i\beta_i = \alpha\,(c_r + ic_i)$$

hence

$$\psi(x,y,t) = \varphi(y)\, e^{\alpha c_i}\, e^{i\alpha(x-c_r t)}$$

It is seen from equation (10) that for large values of Reynolds number, the right side of the Sommerfeld equation becomes very small. Hence, in the limit $R \longrightarrow \infty$ the frictionless perturbation equation

$$(u-c)\ (\varphi''-\alpha^2\varphi) - u''\varphi = 0 \qquad (11)$$

remains.

Experimental evidence shows that instability of laminar flow can only be expected for large Reynolds numbers. Since a general solution of equation (10) is difficult, the method of solving the "eigenvalue" problem is to seek asymptotic solutions of equation (10) for large R. Equation (11) can be taken as limiting case for $R \longrightarrow \infty$. But here there occurs a difficulty due to the fact that in equation (11) the term of highest order φ^{IV} is neglected. Hence it has to be shown that solutions of equation (11) correspond to true asymptotic solutions of equation (10). Furthermore, it can be generally shown that the phase velocity c_r is always smaller than the maximum value of $u(y)$. Consequently, there exists a singularity of equation (11) at the point $y = y_c$ where $u - c_r = 0$ if $u'' \neq 0$.

In the first attempts at solution by Rayleigh (reference 6), only equation (11) was considered. The singularity was avoided by approximating the profile $u(y)$ by a polygon. The result of Rayleigh's investigation was that profiles where u'' changed sign were unstable. Since in equation (10) the influence of friction on the perturbation is neglected, a dynamic instability for certain profiles was thus found. Tollmien (reference 7) has shown that Rayleigh's result was not due to the approximations of the continuous profile by a polygon, and that the change in sign of u'' is a sufficient condition for dynamic instability. Hence, profiles where u'' changes sign are always found to be dynamically unstable.

Prandtl (reference 20) and Tietjens (reference 21) investigated the influence of friction on dynamically unstable profiles. The influence of viscosity was restricted to a small layer close to solid walls: The profile was again approximated by a polygon. Prandtl and Tietjens found that the influence of friction was destabilizing; profiles found dynamically stable became unstable if friction was taken into account. The discovery of this viscous instability is of great importance in view of the fact that experimental evidence shows that viscosity is a decisive factor in the development of turbulence. However, Prandtl and Tietjens' result gave instability for all Reynolds numbers, which does not agree with experimen-

tal results. Tollmien (reference 11) extended Prandtl and Tietjen's work by considering a continuously curved profile. In this case viscosity has to be taken into account close to solid surfaces and in the neighborhood of the singularity of equation (11).

Tollmien investigated an approximation to the Blasius profile and found instability for a small range of frequencies above a certain critical Reynolds number. Schlichting (reference 12) extended Tollmien's theory and computed the amplification, the amplitude distribution, and so forth, of the "dangerous" frequencies. Tollmien's results were not generally accepted since there was no experimental evidence that frequency and wave length, rather than amplitude, bring about the breakdown of the laminar layer and since regular waves, such as should be expected according to the theory, were not observed experimentally. Furthermore, the method of joining the solutions of equation (11) with the solutions of equation (10) in the neighborhood of the singularity was considered mathematically not convincing.

The discovery of the laminar boundary-layer oscillations by Dryden, Schubauer, and Skramstad (reference 14), and the agreement of the measured characteristics of these oscillations with the theoretical results of Tollmien and Schlichting prove the validity of Tollmien's assumptions. Hence, the mechanism of laminar boundary-layer instability on the flat plate can be considered known.

The effect of curvature on disturbances of the form of equation (8) was theoretically investigated by Schlichting (reference 22), who considered the flow in a rotating cylinder using the same general method as Tollmien. Schlichting found a slightly stabilizing effect of curvature (only convex curvature was considered) on the viscous instability. Görtler (reference 9) investigated the influence of both concave and convex curvature on dynamic instability with respect to two-dimensional disturbances (equation(8)). He obtained the result, that velocity profiles where $u'' + \frac{u'}{r}$ changes sign are unstable (r positive for convex, negative for concave curvature).

Since for boundary-layer profiles in the absence of a pressure gradient $u'' \leq 0$, $u' \geq 0$, it follows that a profile which is dynamically stable for two-dimensional perturbations on concave and flat walls can be dynamically unstable on convex walls. This effect, therefore, is in

direct opposition to the simple considerations of Rayleigh and Prandtl. (See sec. IV.)

It is interesting to note that both Tollmien's criterion for dynamical instability, $u'' = 0$, and Görtler's criterion for curved flow, $u'' + \frac{u'}{r} = 0$, correspond to the statement that, if the vorticity has a maximum within the layer the motion is unstable with respect to perturbations of the form (equation (8)).* This suggests that the dynamic instability of the two-dimensional perturbations is due to vortex forces. It will be seen later that the Rayleigh-Prandtl consideration agrees with computations regarding instability with respect to perturbations of the form (equation (9)). Since the direction of the perturbation vorticity of equation (9) is essentially normal to the mean vorticity, little effect of vortex interaction should here be expected.

(β) The three-dimensional perturbation (equation (9)) was first studied by G. I. Taylor (reference 8) in his investigations of the flow in rotating cylinders. Görtler (reference 10) computed the stability of curved boundary-layer flow with respect to these three-dimensional vortices.

For $r >> \delta$, neglecting terms $(\delta/r)^2$ and higher, and neglecting all changes with x, the boundary-layer equations and the continuity equation become:

$$\begin{aligned}
\frac{\partial u}{\partial t} + v\frac{\partial u}{\partial y} + w\frac{\partial u}{\partial z} &= \nu\left\{\frac{\partial^2 u}{\partial y^2} + \frac{\partial^2 u}{\partial z^2}\right\} \\
\frac{\partial v}{\partial t} + v\frac{\partial v}{\partial y} + w\frac{\partial v}{\partial z} + \frac{u^2}{r} &= -\frac{1}{\rho}\frac{\partial p}{\partial y} + \nu\left\{\frac{\partial^2 v}{\partial y^2} + \frac{\partial^2 v}{\partial z^2}\right\} \\
\frac{\partial w}{\partial t} + v\frac{\partial w}{\partial y} + w\frac{\partial w}{\partial z} &= -\frac{1}{\rho}\frac{\partial p}{\partial z} + \nu\left\{\frac{\partial^2 w}{\partial y^2} + \frac{\partial^2 w}{\partial z^2}\right\} \\
\frac{\partial v}{\partial y} - \frac{v}{r} + \frac{\partial w}{\partial z} &= 0
\end{aligned} \tag{12}$$

---

*$u'' + \frac{u'}{r} = 0$ expresses the condition of maximum vorticity if terms with $1/r^2$ are neglected, as is essentially done in Görtler's work.

Putting

$$u = u(y) + u'$$

$$v = v'$$

$$w = w'$$

where u', v', w' are given by equation (9), and putting the pressure

$$P = p(y) + \gamma_4(y) \cos(\alpha z)\, e^{\beta t}$$

equation (12) becomes

$$\begin{aligned}
\beta\gamma_1 + \gamma_2 \frac{du}{dy} &= \nu \left\{ \frac{d^2\gamma_1}{dy^2} - \alpha^2\gamma_1 \right\} \\
\beta\gamma_2 + \gamma_1 \frac{2u}{r} + \frac{1}{\rho}\frac{d\gamma_4}{dy} &= \nu \left\{ \frac{d^2\gamma_2}{dy^2} - \alpha^2\gamma_2 \right\} \\
\beta\gamma_3 - \frac{\alpha}{\rho}\gamma_4 &= \nu \left\{ \frac{d^2\gamma_3}{dy^2} - \alpha^2\gamma_3 \right\} \\
\gamma_3 &= -\frac{1}{\alpha}\frac{d\gamma_2}{dy}
\end{aligned} \tag{13}$$

Eliminating γ_3 and γ_4 from equation (13), one obtains

$$\begin{aligned}
\nu \frac{d^2\gamma_1}{dy^2} - (\beta + \nu\alpha^2)\,\gamma_1 &= \gamma_2 \frac{du}{dy} \\
\nu \frac{d^4\gamma_2}{dy^4} - (\beta + 2\nu\alpha^2)\frac{d^2\gamma_2}{dy^2} + \alpha^2(\beta + \nu\alpha^2)\,\gamma_2 &= -\frac{2\alpha^2 u}{r}\gamma_1
\end{aligned} \tag{14}$$

These simultaneous equations together with the boundary conditions again present an "eigenvalue" problem for α, β, r, and a characteristic Reynolds number. The sign of β determines stability or instability; $\beta = 0$ corresponding to the stability limit. Görtler transforms equation (14) into integral equations and obtains the approximate eigenvalues by means of the method of determinants.

The main results of his analysis can be summarized as follows:

(1) Curvature and Reynolds number enter only in the combination $R_\delta \sqrt{\frac{\delta}{r}}$

(2) Instability - that is, positive values for β - are only possible on concave walls.

(3) Instability on concave walls occurs above a certain critical value of $R_\delta \sqrt{\frac{\delta}{r}}$ for a limited range of the parameter $\alpha\delta$; that is, the ratio of wave length to boundary-layer thickness.

(4) Görtler applies his method to various velocity profiles including the straight-line profile and one profile having an inflection point. He finds the instability region little affected by the shape of the basic profile if the momentum thickness ϑ is taken as the characteristic length.

Görtler's work on the stability of boundary layers with respect to the Taylor vortices (equation (9) considers a dynamic instability without neglecting viscosity. The results therefore differ from the investigations concerning the dynamic instability of the two-dimensional perturbation (equation (8)) of Tollmien's (reference 7) and Gortler's (reference 9) extension to curved flow, where viscosity is neglected entirely and therefore no critical Reynolds number obtained. The difference in the role which viscosity plays in the dynamic instability computed with inclusion of viscous forces, and in the true viscous instability of Tollmien, can be seen from the computed stability limit in these two cases (figs.14 and 15). For increasing R, Görtler's instability region increases; Tollmien' becomes smaller.

For the limit $R \longrightarrow \infty$ Tollmien's instability vanishes; Gortler's, however, does not. A very interesting and important theoretical problem would be the investigation of dynamic instability with respect to the plane disturbance (equation (8)) including the influence of viscosity.

The main result of Tollmien's theory, which can be checked experimentally, is evident from figure 14: Assume that a plane disturbance of a given frequency is excited at some distance from the leading edge of the plate. At a given mean speed the parameter $\frac{\beta r \nu}{U^2}$ and the Reynolds number $R_{\delta_1^*}$ corresponding to f and x, respectively, are

thus given (fig. 14). This wave, traveling at constant frequency downstream, describes a straight line parallel to the R_δ^* axis in figure 14. The Tollmien theory predicts that this wave should decrease in amplitude from $(R_\delta^*)_1$ to $(R_\delta^*)_2$, increase in amplitude from $(R_\delta^*)_2$ to $(R_\delta^*)_3$ and again decrease for $R_\delta^* > (R_\delta^*)_3$.

Görtler's vortex theory for concave walls gives an analogous result. Since in Görtler's theory the wave length is the characteristic quantity, assume a vortex of a given wave length originating at a point corresponding to $\left(R_\vartheta \sqrt{\frac{\vartheta}{r}}\right)_1$ in figure 15. This vortex traveling downstream describes the line A-B in the diagram (fig. 15). Again damping will occur from $\left(R_\vartheta \sqrt{\frac{\vartheta}{r}}\right)_1$ to $\left(R_\vartheta \sqrt{\frac{\vartheta}{r}}\right)_2$; from $\left(R_\vartheta \sqrt{\frac{\vartheta}{r}}\right)_2$ the amplitude will increase till the vortex leaves the instability zone at $\left(R_\vartheta \sqrt{\frac{\vartheta}{r}}\right)_3$.

2. Experimental Results

The discovery of regular oscillations in the laminar boundary layer by Dryden, Schubauer, and Skramstad gave the impulse for a closer study of velocity fluctuations in the laminar layer. During the investigation of the flow past the flat plate, only sporadic appearances of regular fluctuations close to transition were observed. No measurements of frequency, and so forth, were carried out. On the convex side of the r = 20-foot plate, however, the regular wave was observed without any difficulty. The velocity fluctuations for a distance of about 1 foot upstream of the beginning of transition had the appearance of regular sinusoidal waves, increasing in amplitude downstream. These fluctuations are the "natural" excited boundary-layer oscillations discussed by Schubauer and Skramstad (reference 14).

These natural oscillations are excited by disturbances in the free stream. They depend not only on the magnitude but also on the frequency distribution in the free-stream turbulence or noise level. This is probably the reason for the discrepancy between the Reynolds number of transition on the flat plate as found in this research as compared

with Schubauer and Skramstad's values for the same turbulence level. The frequency distribution depends on factors like the number of propeller blades, the revolutions per minute, and so forth, and therefore it is very probable that the distribution in the GALCIT tunnel is quite different from the one in the N.B.S. tunnel. Hence, it seems possible that transition in the GALCIT tunnel was precipitated due to an unfavorable frequency distribution in the external disturbance level. Spectrums of the noise obtained with a sound analyzer showed pronounced maximums in the range of dangerous frequencies.

The frequency of these oscillations could be measured by analyzing the hot-wire output with a sound analyzer or by direct comparison of the hot-wire output with the output of a calibrated electric oscillator on the oscilloscope screen. In agreement with the N.B.S. results, it was found that the measured frequencies followed closely the upper stability limit of Tollmien.* To study the characteristics of the wave more closely and to investigate whether the stability zone on the convex plate agreed with the results of the N.B.S. on the flat plate, several methods of exciting the wave artificially were employed.

(a) A lattice of from four to six thin (0.006-in. diameter) wires stretched at regular intervals normal to the direction of the flow over the surface of the plate was first used to excite the oscillations. Very regular waves could be obtained with this regular roughness. Figure 16 shows some of these regular fluctuations excited with the wire lattice. The frequency of these fluctuations could be easily measured and compared with Tollmien's stability limit. Figure 17 shows the result of these measurements. It is seen that all observed frequencies which show increasing amplitude fall within the Tollmien-Schlichting instability zone or closely beyond the upper limit. In two cases it was possible to measure the frequency of a wave in the stable region, that is, a wave which was excited by the lattice and died out in the stable region; these two points are marked "stable" in figure 17.

Attempts to measure the wave length of the wave were made in the following way: Two hot wires were mounted at

---

*A detailed discussion of these laminar oscillations is given in Schubauer and Skramstad's paper. Therefore, only results where either the flow conditions or the technique of observation differs from the Schubauer and Skramstad research are presented in detail.

NOT REPRODUCIBLE

the same distance from the plate ($\Delta y = 0$) at a distance of 3 centimeters from each other ($\Delta z = 3$ cm). One of the wires was held at a fixed distance x from the leading edge (and hence, from the lattice), the other was moved along on the carriage. A plane wave traveling along x should give a definite correlation between the output of these wires, depending on the ratio $\frac{\Delta x}{\lambda}$, where Δx denotes the distance between the wires, λ the wave length of the oscillation. Figure 18 shows two oscillograms of the two hot-wire outputs for $\frac{\Delta x}{\lambda} = 1$ and $\frac{\Delta x}{\lambda} = 1/2$. The difference in phase is clearly visible. This method can be used to determine the wave length of the disturbance.*

The method of exciting the oscillation with the wire lattice is not well suited for an exact study of the stability limit since the excited frequency cannot be controlled at will. It does, however, show that roughness elements can excite these plane waves in the boundary layer, that these waves increase in amplitude when traveling through the instability region, and that they finally will lead to transition if the amplification is sufficiently large. This influence of roughness on transition led to a somewhat more detailed study of the influence of a single roughness element on the laminar layer. The results of this investigation are presented later on.

With respect to the effect of curvature on transition, the results obtained with the wire lattice show that the mechanism of laminar instability on the convex side of the $r = 20$ foot plate is the same as Schubauer and Skramstad found for the flat plate. Figure 17 shows further that the stability limit for the curved plate cannot differ very much from the limit found on the flat plate.

(b) The method of Schubauer and Skramstad was next used to obtain more exact data regarding the stability limit of Tollmien-Schlichting waves on the curved wall: A phosphor-bronze ribbon about 12 inches long, 1/8 inch wide, and 0.004 inch thick was soldered to thin piano wire

---

*It is naturally possible to determine the correlation coefficient in the conventional manner by adding and subtracting the hot wire outputs before the amplification. However, the method here presented gives a somewhat clearer visualization.

and stretched normal to the flow over the surface of the plate. Two paper spacers about 10 inches apart kept the ribbon at a distance of a few thousandths of an inch from the surface of the plate. An electromagnet mounted on the concave side of the plate produced a fairly strong magnetic field in the center of the ribbon. The output of an electrical oscillator was fed over a power amplifier into the ribbon and thus gave rise to forced oscillations of the ribbon in the magnetic field.

The frequency of the ribbon-excited boundary-layer oscillation could be measured in the same way as in the case of the natural oscillations and the waves from the wire lattice. The wave length, however, could be obtained in a much simpler way: The output of the oscillator which drove the ribbon was connected to the horizontal; the hot-wire output, to the vertical deflection plates of a cathode ray oscilloscope. Hence, the phase shift between the ribbon oscillation and the velocity fluctuation picked up by the hot wire is a function of the ratio of the distance Δx between ribbon and hot wire and the wave length λ of the wave. The Lissajou figure on the oscilloscope screen will therefore change periodically when the wire is moved along x and repeat itself every time the wire is shifted one wave length. Hence, the measurement of the wave length requires only one hot wire and a measurement of a length. If the frequency f and the wave length λ are known, the parameters $\frac{\beta_r \nu}{U^2}$, $\alpha\delta^*$, $\frac{c_r}{U}$ of the Tollmien-Schlichting theory can be computed. To coordinate the results with the instability zone the amplification of the oscillation downstream from the ribbon has to be investigated. This was done by measuring the amplitude of the fluctuation with the hot wire at various distances downstream from the ribbon. Figure 19 shows a typical result. The relative fluctuation amplitude for several frequencies is plotted as a function of the distance from the ribbon. It is seen that some frequencies increase in amplitude downstream. The amplitudes of the fluctuations with $f = 250$ and $f = 300$ first increase and then decrease, the fluctuation with $f = 50$ first decreases and then increases in amplitude. Hence, the extremes of this diagram denote the stability limit: the Reynolds number $R\delta^*$, corresponding to a minimum of amplitude, together with the frequency parameter $\frac{\beta_r \nu}{U^2}$ for the respective frequency, determine one point on the lower stability limit of figure 14. Maximums determine points on the upper stability limit.

(c) During the investigation of the effect of a single roughness element on the laminar layer (see sec. VII), it was noticed that sound waves had a pronounced effect on the unstable inflection-point profiles prevailing in the wake of the obstacle. Hence, the roughness element together with a loud-speaker can be used in place of the vibrating ribbon. A few measurements have been made with this device. However, the method is limited to low Reynolds numbers since at higher Reynolds numbers transition takes place in the wake of the obstacle.

Figures 20 to 22 show the results obtained from measurements on the convex side of the $r = 20$-foot plate. It is seen that the results agree well with the measurements of the N.B.S. on the flat plate. A slight shift of the stability region toward higher values of R_{δ^*} hardly exceeds the scatter. Measurements of the stability limit on the convex side of the $r = 30$-inch plate were also made. The region near the critical Reynolds number was chiefly investigated to check if the slight shift in the stability limit was again present. Figures 23 to 25 show the results. The shift toward higher R_{δ^*} as compared with the N.B.S. results is again noticeable.

The influence of curvature on the stability limit is so small that it is a posteriori justified to plot the results of all measurements on one curved plate together in spite of the fact that, since different points were measured at different boundary-layer thicknesses, the parameter δ/r is not the same for all points. Within the accuracy of measurement, this difference can be neglected; hence the measurements on the $r = 20$-foot plate and on the $r = 30$-inch plate can be considered as measurements with $\frac{\delta}{r} \doteq 10^{-4}$ and $\frac{\delta}{r} \doteq 10^{-3}$, respectively. A comparison of these results with the computations of Schlichting (reference 22) regarding the influence of curvature on the Tollmien instability is somewhat difficult, since Schlichting's basic velocity profile is not the same as that of Tollmien. Hence, the absolute magnitude of the critical Reynolds number is different (for $\frac{\delta}{r} = 0$ the flat plate, Schlichting finds $R_{\delta^*_{cr}} = 1530$ as compared with Tollmien's value of 420). However, the relative influence of curvature on the critical number can be compared: The critical Reynolds number for the $r = 30$-inch

plate where the instability limit is more accurately measured than on the $r = 20$-foot plate is about $R_{\delta^*_{cr}} = 600$ as compared with $R_{\delta^*_{cr}} = 450$ measured by Schubauer and Skramstad on the flat plate. Schlichting (reference 22) finds at $\frac{\vartheta}{r} = 0$, $R_{\delta^*_{cr}} = 1530$ and at $\frac{\vartheta}{r} = 0.004$, $R_{\delta^*_{cr}} = 1960$. Linear interpolation thus gives for $\frac{\vartheta}{r} \doteq 0.001$, $R_{\delta^*_{cr}} = 1640$. Hence, the shift in the critical number is of the same order. Further conclusions cannot be drawn since the experimental accuracy in determining the lower instability limit is very poor and since the velocity profile in the theory differs from the one met in the experiment.

A detailed investigation of flow past a concave wall has not yet been carried out. Hence, an experimental check of Görtler's stability limit similar to the investigation of the Tollmien-Schlichting wave cannot yet be given. However, a few conclusions based on measurements on the concave side of the $r = 20$-foot plate can be given here:

(a) The Tollmien-Schlichting waves were not observed on the concave side of the $r = 20$-foot plate

(b) The critical parameter of Görtler's theory is $R_\vartheta \sqrt{\frac{\vartheta}{r}}$. If the measurements presented in figure 11 are replotted so as to give $\left(R_\vartheta \sqrt{\frac{\vartheta}{r}}\right)_{tr}$ against $\frac{\vartheta}{r}$ instead of $R_{\vartheta_{tr}}$ against $\frac{\vartheta}{r}$, it is seen from figure 26 that $\left(R_\vartheta \sqrt{\frac{\vartheta}{r}}\right)_{tr}$ is closely constant for all $\frac{\vartheta}{r}$ measured; only for the smallest values of $\frac{\vartheta}{r}$ does $\left(R_\vartheta \sqrt{\frac{\vartheta}{r}}\right)_{tr}$ decrease. This latter decrease is expected since $R_{\vartheta_{tr}}$ for $\frac{\vartheta}{r} = 0$ has to have a finite value. The absolute value of $R_\vartheta \sqrt{\frac{\vartheta}{r}}$ at transition is appreciably larger than Görtler's stability limit; $R_\vartheta \sqrt{\frac{\vartheta}{r}} \doteq 7.3$ at transition as compared with $R_\vartheta \sqrt{\frac{\vartheta}{r}} = 0.58$, the theoretical critical number. This, however, is no discrepancy between theory and experiment, since the limit of stability means only that certain vortices can be amplified from here on. Transition, however, means that the perturbations become large enough to cause a complete

breakdown of orderly laminar flow. This difference is exactly the same in the flow along a flat plate where the stability limit of the Tollmien-Schlichting wave is about $R_{\delta^*_{cr}} = 450$ but the layer can remain laminar up to values of R_{δ^*} of the order of 3000.

(c) A third argument which supports the assumption that transition on concave walls is caused by Taylor-Görtler vortices is given in the discussion of the effect of angle of attack later on.

The results of the experimental investigation of boundary-layer stability agree and support the results found for the transition point: Transition is little affected by convex curvature in the investigated range from $\frac{\vartheta}{r} = 0$ to $\frac{\vartheta}{r} \doteq 0.001$ because the Tollmien-Schlichting waves which bring about the breakdown of the laminar layer are only slightly affected by curvature. Transition is affected by concave curvature because, in addition to the Tollmien-Schlichting wave, a strong dynamic instability enters. To give an idea of the magnitude of this destabilizing effect of concave curvature, consider an airfoil of camber K with a chord S. The radius of curvature of the airfoil is approximately:

$$r = \frac{1}{8}\frac{S}{K}$$

Neglecting the influence of pressure gradient, the maximum momentum thickness of the boundary layer is

$$\vartheta = \frac{2}{3}\sqrt{\frac{\nu S}{U}}$$

or

$$R_\vartheta^2 \frac{\vartheta}{r} \doteq 2.5\, K\sqrt{\frac{US}{\nu}}$$

Transition was found to occur for $R_\vartheta^2 \frac{\vartheta}{r} \doteq 50$

hence

$$K\sqrt{R_s} \doteq 20$$

For example, with 2-percent camber, the Reynolds number above which the curvature effect determines transition is

$$R_s \doteq 10^6$$

Hence, it is seen that under certain conditions concave curvature can have a strong influence on transition. It must be pointed out, of course, that most modern airfoils have no concave curvature where the boundary layer would be laminar.

This is obviously only a crude estimate. To neglect the influence of pressure gradient on transition on concave walls is, however, probably not so far off as a similar assumption for flat or convex boundaries. The stability limit of concave flow with respect to the three-dimensional vortices was found little affected by the shape of the velocity profile. Hence, the pressure gradient will influence the three-dimensional instability very little. Only if the gradient becomes so large that transition is precipitated, due to the two-dimensional instability, can a large influence of the pressure gradient be expected. The analogous angle-of-attack effect is discussed later on.

VII. SINGLE ROUGHNESS ELEMENT

During the investigation of the Tollmien-Schlichting waves with the wire lattice, it was found that these wires, stretched along the surface of the plate in the boundary layer, in no case caused immediate transition. It was therefore decided to investigate the influence of a single roughness element such as a wire or a narrow strip on the laminar boundary layer. For this purpose, a strip of rubber tape about 1 centimeter wide, 25 centimeters long, and 0.1 centimeter thick was glued directly on the glass plate, thus forming a single two-dimensional roughness element. The velocity profiles downstream from this element, the velocity fluctuations, and the occurrence of transition were then studied. The main purpose of this investigation was to analyze the action of such a disturbance on the laminar layer. The results of this study showed that there exist three primary and readily distinguishable cases. Figures 27, 28, and 29 show a typical example of each.

(1) The inflection-type profiles prevailing in the wake of the obstacle and immediately downstream from it are gradually reduced to the normal Blasius-type velocity profile (fig. 27).

(2) The inflection-type profile still changes to a Blasius profile but the disturbance - that is, the induced laminar waves - are so strong when the Blasius profile is

NOT REPRODUCIBLE

attained that transition occurs almost immediately. This case is seen in figure 28, and it is to be noted that the flow in the wake of the obstacle is still laminar, turbulence occurring only after a Blasius-type profile has been passed through.

(3) Figure 29 finally shows velocity profiles taken in the wake of the obstacle with and without an external disturbance - in this case sound waves. It is seen that the addition of a relatively small external disturbance causes a radical change in the profile. Without the influence of the sound waves, the profile shows the existence of a dead fluid region bounding a laminar wake. The addition of 25 decibels of sound of a rather high frequency (700 cycles) causes transition in the wake and produces a turbulent profile as shown in figure 29.* The radical difference is further illustrated by the record of velocity fluctuations shown in figure 30.

The appearance of these three types of disturbance caused by roughness leads to the following conclusions: Transition caused by a roughness element does not necessarily occur immediately at the element, but may occur at some distance downstream. Furthermore, transition caused by a roughness element may occur in the roughness-element wake proper or further downstream after the layer has returned to a normal Blasius-type profile. This latter fact might cause considerable variation in the turbulent boundary-layer character downstream from the transition point for the following reason: It is known that, if transition takes place in a normal laminar boundary layer, the logarithmic velocity distribution established itself almost immediately after transition. In the language of the mixing-length theory, the turbulent profile corresponds to a mixing length proportional to the distance from the solid boundary. If, however, transition takes place in the wake of the obstacle, the turbulent exchange corresponds to a mixing length proportional to the width of the wake, or the distance from the obstacle. Farther downstream the influence of the solid boundary will become noticeable and, close to the surface, the logarithmic distribution is again to be expected. The profile (c) in figure 29 appears to be of this type.

---

*The same effect could be caused by an increased tunnel turbulence. However, the sound was simpler to apply.

Further research is required to determine how a turbulent velocity profile of this type develops. It seems interesting to note that the profile (c) in figure 29 bears a close resemblance to velocity profiles found to exist shortly before turbulent separation takes place. It is conceivable that this resemblance is not wholly accidental but that the turbulent mechanism is similar in both cases: namely, a region of "wall-turbulence" and an outer region of "free turbulence." This, in fact, is certainly to be expected if the turbulent layer develops from a separated laminar layer since this case would be similar to the flow behind an obstacle.

Which of the three cases above-described actually occurs will depend on a critical Reynolds number, and in addition, on the level and the frequency spectrum of external disturbances, such as the turbulence of the free stream or noise. The critical number for a roughness element in a laminar boundary layer is usually considered to be given by the height ϵ of the element and the velocity which exists at this height in the undisturbed layer. In the case of a Blasius profile, this leads to

$$R_\epsilon \sim R_x^{3/2} \left(\frac{\epsilon}{x}\right)^2$$

if the element is small enough to consider the profile as linear near the wall. Goldstein (reference 23) gives as critical number $(R_x)^{3/2} \left(\frac{\epsilon}{x}\right)^2 \leq 150$ and 90 for round or sharp elements, respectively. The corresponding Reynolds number for the first case (fig. 27) was computed from the experimental data as approximately 500 - that is, at a considerably larger Reynolds number than Goldstein's critical values, the flow still remains laminar. This difference is at least partially due to the unusually low turbulence level in the free stream for the present investigation and the consequent greater stability of the laminar wake of the obstacle. The critical number for case 2 (fig. 28) is 2000, and as pointed out before, the roughness element wake is still laminar. Case 3 (fig. 29) finally shows that (at Reynolds number = 1300) the wake can be rendered turbulent by an external disturbance.

The Reynolds number R_ϵ and the turbulence level (or any other external disturbance) determine the stability of the roughness element wake. In addition, a second

critical number has to be considered which determines the stability of the laminar boundary layer to which the flow may return downstream from the wake proper. If this Reynolds number R_{δ^*} is smaller than the Reynolds number corresponding to the lower limit of the Tollmien-Schlichting instability region (see fig. 13) the disturbances induced by the roughness element will die out; if R_{δ^*} is larger, part of the disturbances will be amplified and will eventually lead to transition.

VIII. INFLUENCE OF THE PRESSURE GRADIENT ON BOUNDARY-LAYER TRANSITION

The influence of the pressure gradient on boundary-layer transition along the convex side of the 20-foot radius of curvature plate was studied. Figure 31 shows the pressure distributions for which transition was measured. It is seen that the waviness of the distribution remains unaltered when the mean slope is changed. This confirms the statement made above that the waves in the distribution are due to small local changes in radius of curvature. Measurements of transition with the pressure distribution A have already been discussed. The results obtained with the distribution B are shown in figure 32. These results were somewhat surprising; although the transition Reynolds numbers were found to be smaller than expected, they failed to indicate any noticeable dependency on x. Furthermore, no systematic influence of the waves in the pressure distribution was noted on the critical Reynolds number. The only effect of these pressure-distribution waves was found in the length of the transition region - that is, the region between the appearance of the first turbulent bursts and the point where the layer appears fully turbulent. This region was short when the pressure increased, and lengthened when it decreased. A few of the measured regions showing this effect are included in figure 32.

With the pressure distribution C (fig. 33) the transition Reynolds number was found to decrease still further (fig. 33), and here the critical number was found to depend on x (or δ). It is seen from figure 33 that $R_{x_{tr}}$ decreases with increasing x from a value of 1.3×10^6 at x = 70 centimeters to a value of about 0.5×10^6 at

$x = 160$ centimeters. A slight decrease is also seen at values of x less than 70 centimeters. However, this latter decrease does not mean too much since this point had to be measured at the highest obtainable speeds of the tunnel and at this speed, the turbulence level of the free stream increases.*

Since the pressure distribution C was reasonably close to a linear distribution, the separation point could easily be computed using the Kármán-Millikan or the simplified von Doenhoff procedure. The latter computation gave $x_s = 140$ centimeters. Unfortunately, this is too close to the trailing edge of the plate to permit a study of the flow after separation in detail and with the present set-up, it was impossible to obtain higher gradients. A series of velocity profiles was then measured in order to check the computed separation point. However, owing to the relatively small gradient, the change in the velocity profile was so gradual that a satisfactory determination of the separation point was not possible. As an example, figure 34 shows two velocity profiles at $x = 30$ centimeters and at $x = 70$ centimeters. It is seen that the profile at $x = 70$ centimeters is already very close to a separation profile.

Finally, measurements were made with the pressure distribution D (fig. 31). The results are shown in figure 35. There is a marked increase in the transition Reynolds number. Because of the limited tunnel velocity, only a few points could be measured. With the pressure distribution C and D the effect of the gradient on the length of the transition region was again noted as with distribution B.

There remains the question as to the proper parameter governing the influence of pressure gradient on boundary layer transition. It is felt that from measurements of the type described above the proper parameter cannot be found for the following reason:

At zero pressure gradient and low free-stream turbulence, the breakdown of laminar flow is caused by the viscous instability waves of Tollmien and Schlichting.

---

*For velocities above 30 m/sec the tunnel turbulence increases from $\frac{u'}{u} = 0.08$ percent to 0.09 percent at 38 m/sec.

If the pressure gradient is positive, two influences will increase the instability: One is the influence of the pressure gradient on the Tollmien-Schlichting wave, the other is the development of a strong dynamic instability due to the change in velocity profile from the Blasius-type profile to a profile having an inflection point. The influence of pressure gradient on the Tollmien-Schlichting wave was studied by Schubauer and Skramstad (reference 14). An increased amplification in the instability zone and a broadening of the zone were found. The effect of the dynamic instability is not yet clear since, as mentioned before, no critical Reynolds number has been computed and the influence of the shape of the profile on the instability is unknown, apart from the general statement that the profile must have an inflection point. The problem bears some resemblance to the curvature effect: On concave walls a strong dynamic instability enters and apparently becomes the determining factor in bringing about the breakdown of the laminar flow. The influence of pressure gradient appears to be of the same nature except that the type of perturbation is the same for viscous and dynamic instability. To determine the parameter governing the influence of pressure gradient on transition will, therefore, require a detailed study of the perturbations leading to the breakdown of the laminar flow.

IX. THE ANGLE-OF-ATTACK EFFECT

It was mentioned before that Schiller (reference 2) and Hall and Hislop (reference 3) found a strong influence of the angle of attack of the plate on the location of the transition point. Based on the theoretical analysis of boundary-layer instability and the foregoing measurements on the influence of the roughness element and pressure gradient, an explanation of this effect can be given.

Assume that the transition point of flat-plate flow is to be investigated and that the measurements are carried out on the side, say A (fig. 36) of the plate. The plate is said to be under a favorable angle of attack if the stagnation point lies on the side A, under an unfavorable angle of attack if the stagnation point lies on B. The boundary layer on A in the latter case has to pass around the leading edge of the plate. Hence, the pressure gradient over the first part of A will be positive and its magnitude will increase as the radius of curvature of the leading edge becomes smaller. In other words, the leading

edge acts like a roughness element for the side A; the initial boundary-layer profile will have an inflection point and thus the same effects as found with the roughness element (see sec. VII) are to be expected. A disturbance in the stream will be amplified because of the instability of the profiles and, if finally the Blasius-type layer develops downstream, the disturbances are amplified in the Tollmien-Schlichting zone and lead to precipitated transition. At very large angles of attack transition can even occur in the wake of the leading edge without a Blasius layer being formed at all. As the plate is turned, the effect will occur very suddenly if the leading edge is a knife edge and more continuously if the edge is rounded, in agreement with the above measurements (reference 5). Setting the plate to zero angle of attack is difficult since, even if the setting were correct for a given mean direction of the flow, the directional velocity fluctuations (v') would complicate the matter. It therefore seems reasonable to avoid this initial dynamic instability by setting the plate to a slight favorable angle of attack. This has, in fact, been done in most recent investigations.

It was mentioned before that Charters investigated the effect of angle of attack of a curved plate to test the validity of Taylor's (reference 4) criticism of the results of the Clausers (reference 1). Charters found that the setting of the plate was critical for the convex but not very critical for the concave side. This effect is understandable if it is assumed that transition on the concave side is brought about by Taylor-Gortler vortices. These vortices were found to depend little on the velocity profile and therefore an inflection point profile would not have much influence, so long as the unfavorable angle of attack is not so large as to cause transition in the wake proper of the leading edge.

X. THE DEVELOPMENT OF TURBULENT FLOW

The preceding parts, both experimental and theoretical, deal mainly with the breakdown of laminar flow. The question as to how the orderly wave or vortex motion changes into the statistically fluctuating turbulent motion is not answered. Schubauer and Skramstad (reference 14) give an excellent review of this problem in connection with their measurement; only little can be added here:

It appears that the formation of eddies starts from some dynamic instability in a manner similar to the breaking of waves or the rolling-up process of a vortex sheet. Hence, the first step in bridging the gap between laminar instability and turbulent motion is to find the development from the orderly motion to a dynamically unstable configuration. The Tollmien-Schlichting wave can bring about such an instability in two ways:

(1) The fluid close to the solid surface will, when the amplitude of the wave becomes sufficiently large, come to rest or actually reverse its motion during one-half period of the oscillation. The "instantaneous" profile is then certainly of the dynamically unstable type. However, the latter conclusion is only correct if the frequency of the perturbation for which this profile is unstable is large compared with the frequency of the Tollmien-Schlichting wave. Only in this case can the instantaneous profile due to the wave be considered a "mean" profile for the dynamic instability. The same argument applies, of course, to Taylor's (reference 13) theory of forced transition due to fluctuating pressure gradients. The experiments with roughness element (see sec. VIII) have shown that separation profiles can prevail for quite some distance downstream and can actually return to a stable form without the development of turbulent flow. On the other hand, there exists some experimental evidence for Taylor's theory of forced transition. A better understanding of the stability of inflection point profiles is needed here for a clear decision.

(2) The u' and v' components of the Tollmien-Schlichting waves have a finite correlation. The correlation coefficient $k = \frac{\overline{u'v'}}{\sqrt{\overline{u'^2}}\sqrt{\overline{v'^2}}}$ reaches a maximum value of $k \doteq -0.2$ as compared with the correlation coefficient in the turbulent boundary layer of $k \doteq -0.3$. There exists, therefore, an apparent shearing stress $\tau = \rho\overline{u'v'} = \rho k\sqrt{\overline{u'^2}}\sqrt{\overline{v'^2}}$ which increases with increasing amplitude of the wave. Owing to this shear the initial profile will be gradually distorted and it appears very probable that the profile becomes dynamically unstable. Since the problem is a typical nonlinear one (the profile being distorted by the wave, the distorted mean profile leads to a change in the wave, and so on); hence, no definite form of the final profile can be given.

In the case of the Taylor-Görtler vortices also, a change of the mean profile due to the vortices must be assumed; in spite of the fact that these vortices are already the result of a dynamic instability. The wave length of these vortices is too large to assume that these develop into turbulent eddies, and furthermore, Pai (reference 24) found that these vortices can exist in turbulent motion. Since Taylor-Görtler vortices do not vary periodically with time only a continuous change in mean profile analogous to case 2 with the Tollmien-Schlichting wave is possible.

However, even tracing the process up to a violent dynamically unstable configuration is only one step forward in the general problem, since the dynamic instability is again only known for small perturbations. The actual development of statistical turbulence appears to be a nonlinear process and still presents a formidable problem for future research.

XI. CONCLUSIONS

The breakdown of laminar flow can be caused by either a dynamic or a viscous instability. The boundary layer on convex surfaces at least up to values of $\frac{\delta}{r} = 0.001$ is dynamically stable but has viscous instability. The viscous instability leads to the development of laminar-boundary-layer oscillations which have been predicted theoretically by Tollmien and Schlichting and were found experimentally by Schubauer and Skramstad on a flat plate. The characteristics of these laminar oscillations are but little influenced by convex curvature in the investigated range from $\frac{\delta}{r} = 0$ to $\frac{\delta}{r} = 0.001$. The Reynolds number of transition is consequently unaltered on convex surfaces as compared with the flat plate. Transition on the upper surface of an airfoil will therefore not be noticeably influenced by the curvature. The results of Milton and Francis Clauser which predicted a strong stabilizing effect of convex curvature are based on the assumption of an identical mechanism of transition on convex and concave walls. This assumption appears not to be correct. The boundary layer on concave surfaces is apparently dynamically unstable with respect to certain three-dimensional vortices. This instability was theoretically predicted by Görtler and measurements of the transition point on a concave surface confirm his theory.

The destabilizing effect of roughness elements and of an adverse pressure gradient on the laminar boundary layer are due to a dynamic instability of inflection point profiles. Theory and experiment are not yet advanced enough to draw definite conclusions as to the governing parameters for roughness and pressure gradient effect. Both effects appear rather complicated owing to the change in the mean velocity profile downstream and the development of dynamic instability in addition to the viscous instability. Transition in the wake of a roughness element can occur in the wake proper of the element - due to the dynamic instability of the inflection point profile in the wake, or after the boundary layer has reattached to the wall. The boundary layer in the latter case returns to the dynamically stable Blasius profile, but laminar oscillations are induced by the unstable wake and these lead to a precipitated breakdown of the laminar layer.

California Institute of Technology,
Pasadena, Calif., June 1943.

REFERENCES

1. Clauser, Milton, and Clauser, Francis: The Effect of Curvature on the Transition from Laminar to Turbulent Boundary Layer. T.N. No. 613, NACA, 1937.

2. Schiller, L.: Neue quantitative Versuche zur Turbulenz Entstehung. Z.f.a.M.M. 14, 1934, pp. 36-42.

3. Hall, A. A., and Hislop, G. S.: Experiments on the Transition of the Laminar Boundary Layer on a Flat Plate. R.&M. No. 1843, British A.R.C., 1938.

4. Taylor, G. I.: Some Recent Developments in the Study of Turbulence. Proc. of the Fifth Int. Cong. for Appl. Mechanics, J. Wiley & Sons, Inc., (New York), 1939.

5. Charters, Alex C., Jr.: Transition between Laminar and Turbulent Flow by Transverse Contamination. T.N. No. 891, NACA, 1943.

6. Rayleigh, Lord.: On the Stability, or Instability, of Certain Fluid Motions I, II. Proc. London Math. Soc. 11, pp. 57-70; 18 and 19, pp. 67-74, 1887.

7. Tollmien, W.: General Instability Criterion of Laminar Velocity Distributions. T.M. No. 792, NACA, 1936.

8. Taylor, G. I.: Stability of a Viscous Liquid Contained between Two Rotating Cylinders. Phil. Trans. Roy. Soc. London ser. A, 223, pp. 289-343, 1923.

9. Görtler, H.: Über den Einfluss der Wandkrümmung auf die Entstehung der Turbulenz. Z.f.a.M.M. 20, pp. 138-147, June 1940.

10. Görtler, H.: Über eine dreidimensionale Instabilität laminarer Grenzschichten an konkaven Wänden. Göttinger Nachrichten. Neue Folge, 2, Nr. 1.

11. Tollmien, W.: The Production of Turbulence. T.M. No. 609, NACA, 1931.

12. Schlichting, H.: Zur Entstehung der Turbulenz bei der Plattenströmung. Göttinger Nachrichten, M.P.K., pp. 181-208, 1933, und Bd. 1, 1935.

13. Taylor, G. I.: Statistical Theory of Turbulence. V - Effect of Turbulence on Boundary Layer. Theoretical Discussion of Relationship between Scale of Turbulence and Critical Resistance of Spheres. Proc. Roy. Soc. London, ser. A, 156, pp. 307-317, Aug. 17, 1936.

14. Schubauer, G. B., and Skramstad, H. K.: Laminar-Boundary-Layer Oscillations and Transition on a Flat Plate. NACA, A.C.R., Apr. 1943.

15. Mock, W. C., Jr., and Dryden, H. L.: Improved Apparatus for the Measurement of Fluctuations of Air Speed in Turbulent Flow. Rep. No. 448, NACA, 1932.

16. Dryden, H. L.: Air Flow in the Boundary Layer near a Plate. Rep. No. 562, NACA, 1936.

17. Peters, H.: A Study in Boundary Layers. Proc. of the Fifth Int. Congr. for Appl. Mechanics, J. Wiley & Sons, Inc., (New York), 1939.

18. Rayleigh, Lord.: On the Dynamics of a Revolving Fluid. Sci. Pap., vol. 6, 1916.

19. Prandtl, L.: Effect of Stabilizing Forces on Turbulence. T.M. No. 625, NACA, 1931.

20. Prandtl, L.: Bemerkungen über die Entstehung der Turbulenz. Z.f.a.M.M. 1, pp. 431-436, Bd. I, Heft 6, Dec. 1921.

21. Tietjens, O.: Beiträge zur Entstehung der Turbulenz. Z.f.a.M.M. vol. 5, no. 3, June 1925, pp. 200-217.

22. Schlichting, H.: Über die Entstehung der Turbulenz in einem rotierenden Zylinder. Göttinger Nachrichten, Heft 2, 1932.

23. Goldstein, S.: Modern Developments in Fluid Dynamics. The Clarendon Press (Oxford), 1938, p. 318.

24. Pai, Shih-I.: Turbulent Flow between Rotating Cylinders. T.N. No. 892, NACA, 1943.

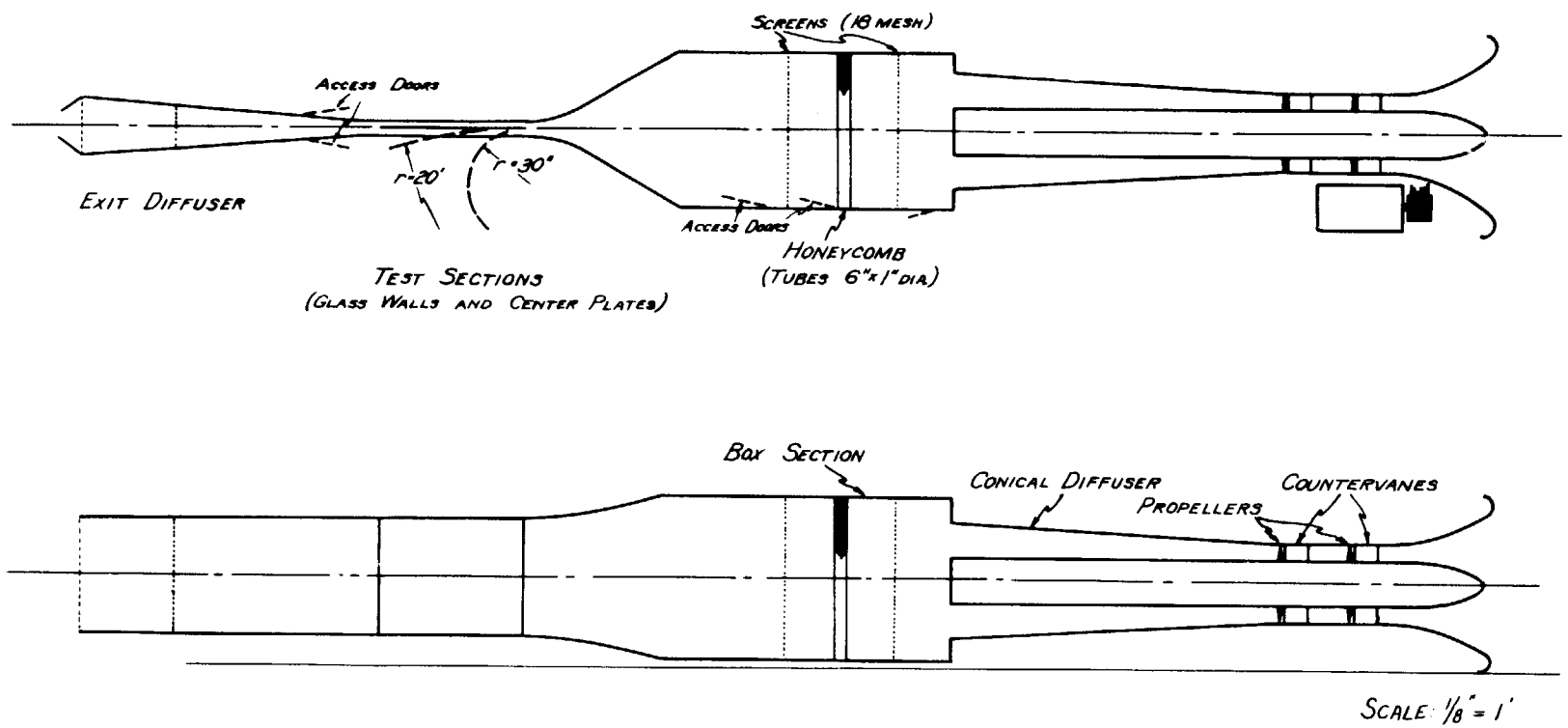

Figure 1.- Flow Diagram of the Boundary Layer Research Tunnel

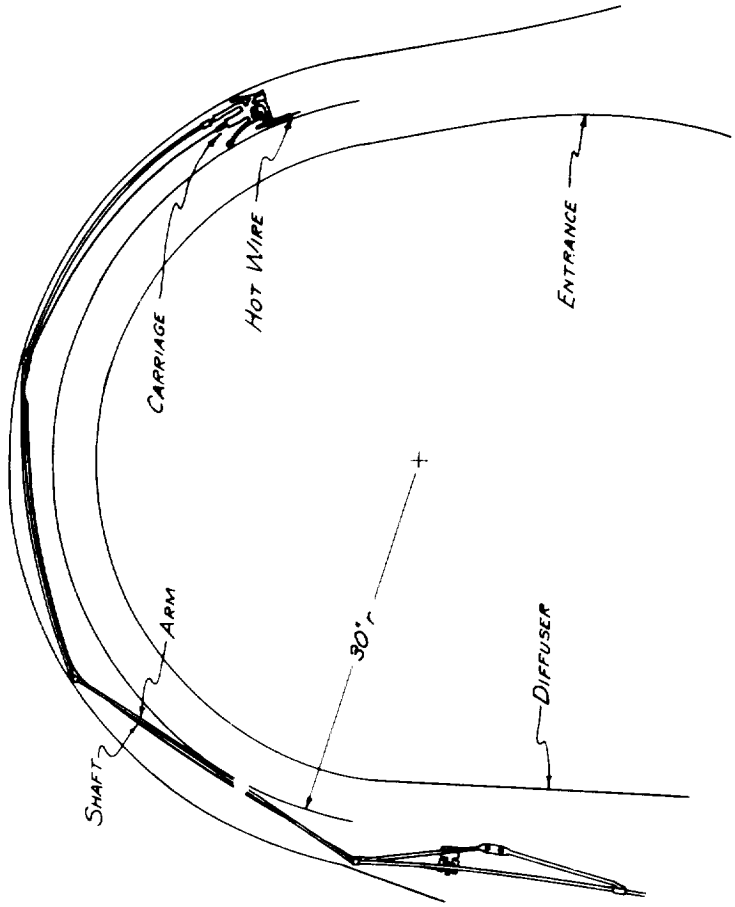

Figure 2.- Schematic diagram of the traversing mechanism.

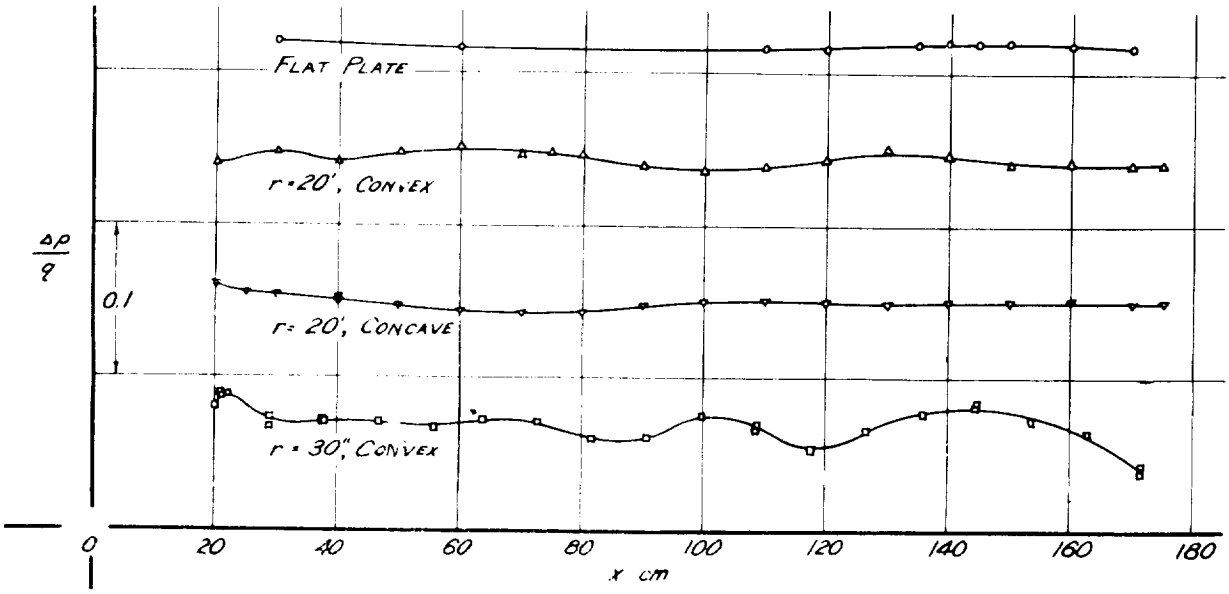

Figure 5.- Pressure distributions along the test plates for "zero" gradient.

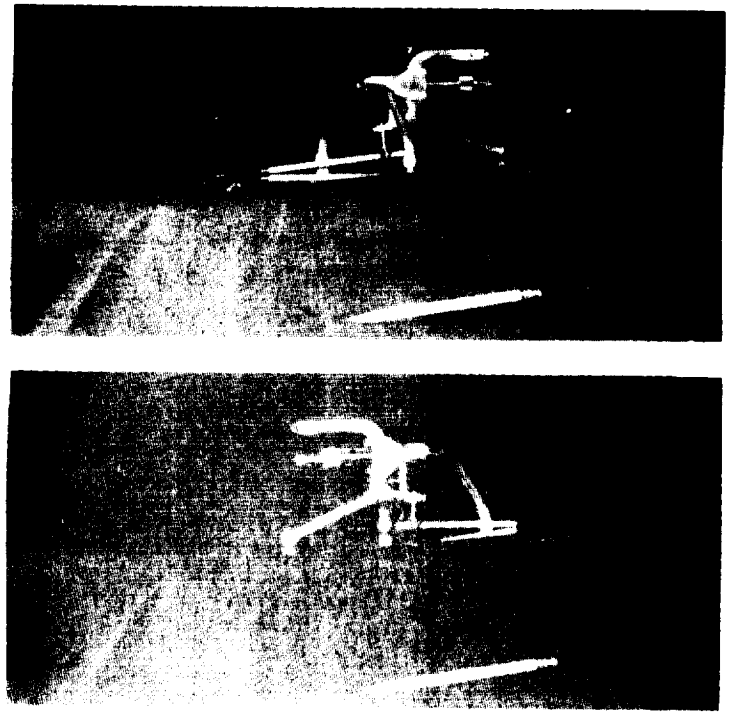

Figure 3.- The instrument carriage.

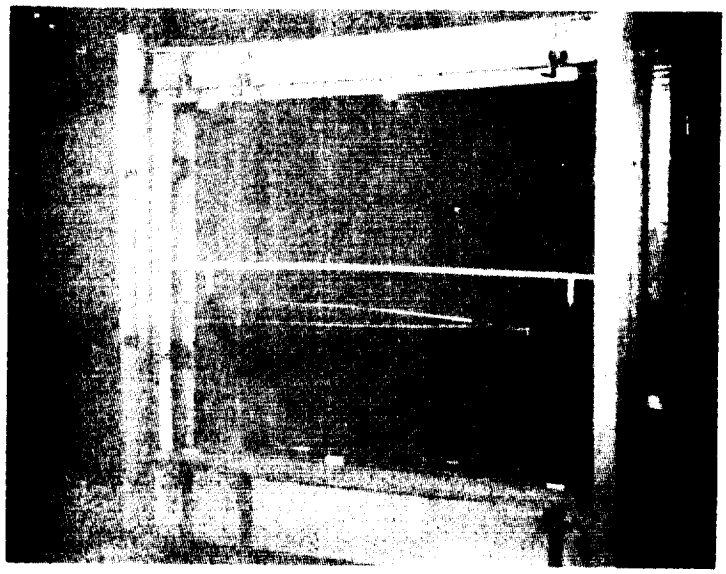

Figure 4.- The test section with 20' radius of curvature.

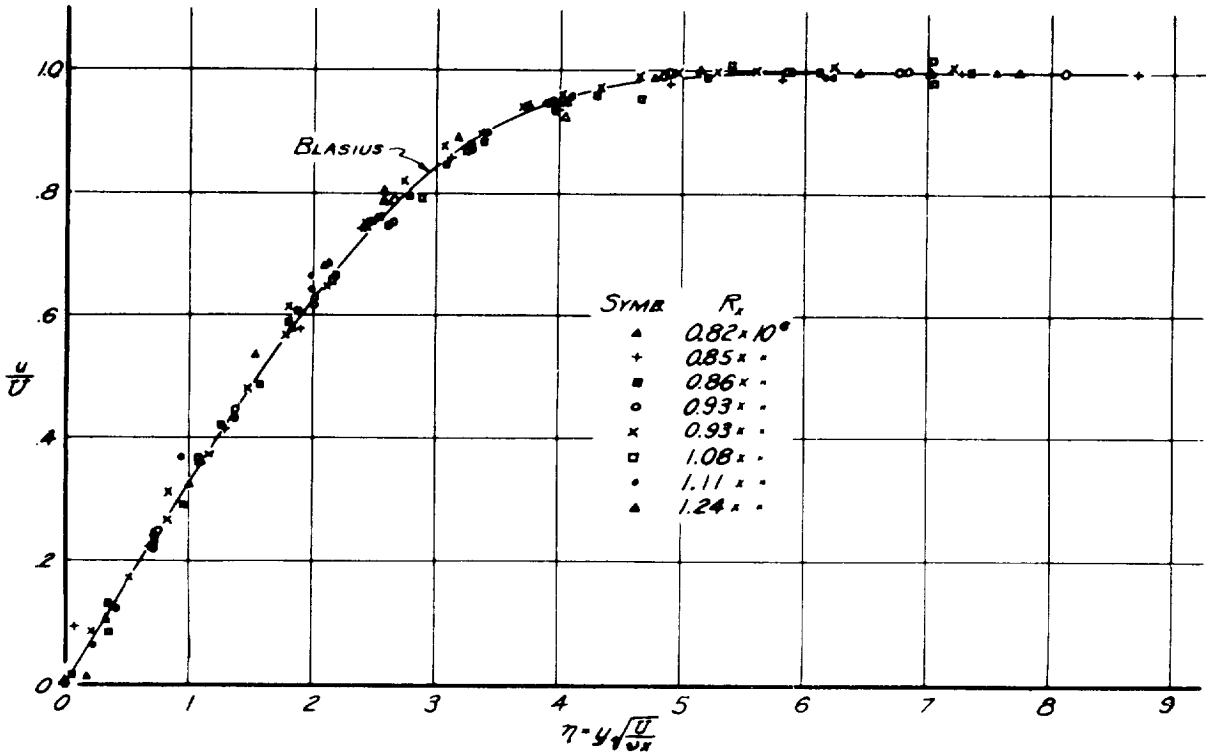

Figure 6.-Velocity distribution in the laminar boundary layer of the flat plate.

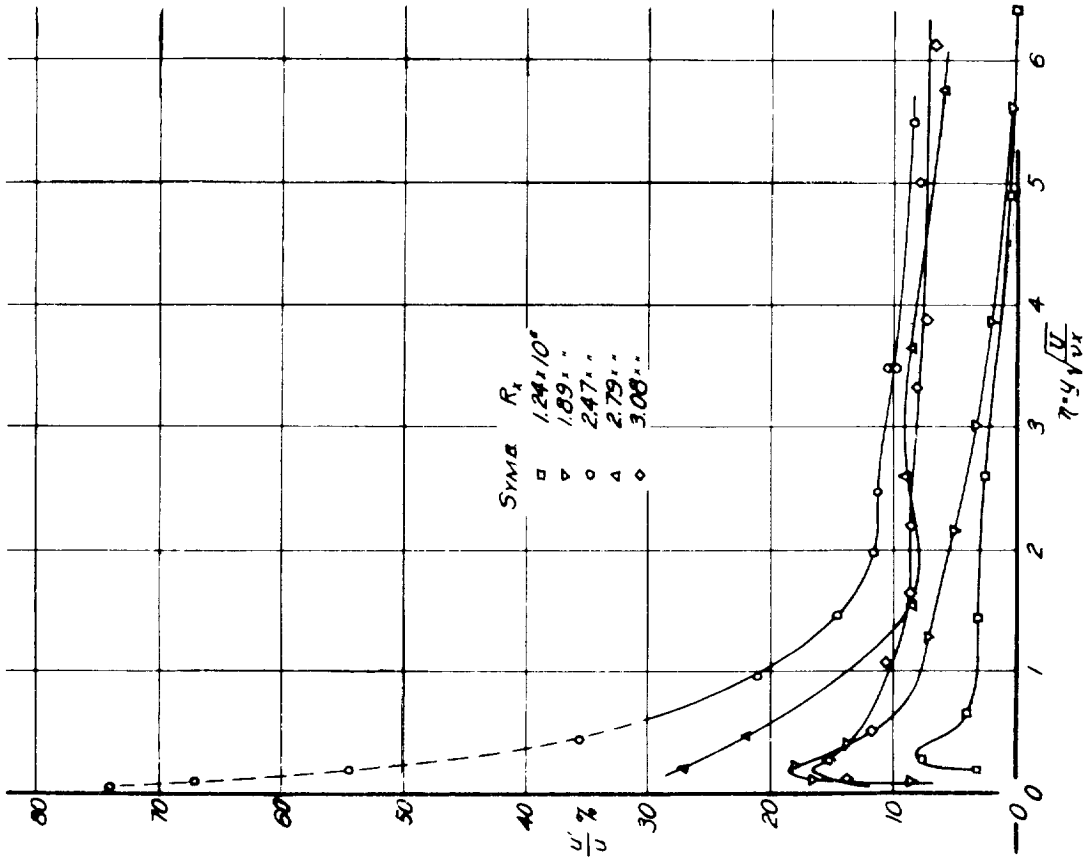

Figure 7.- Distribution across the boundary layer of the velocity fluctuations parallel to the mean flow.

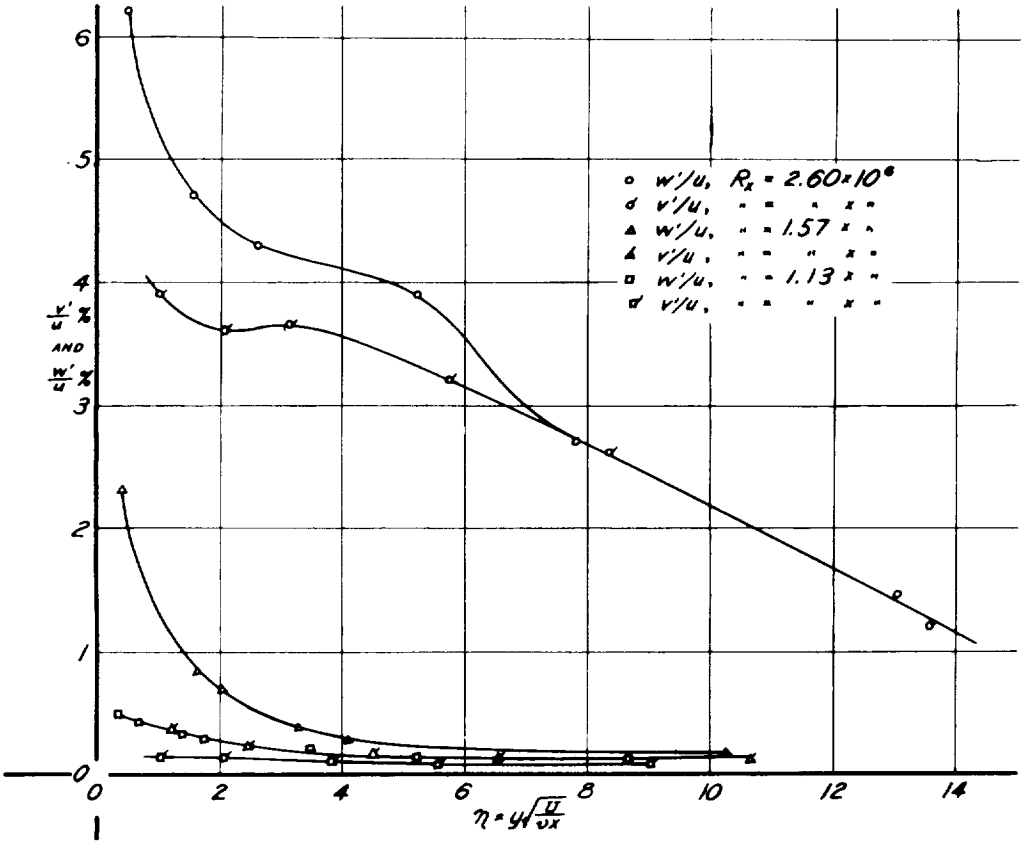

Figure 8.- Distribution across the boundary layer of the velocity fluctuations normal to the mean flow

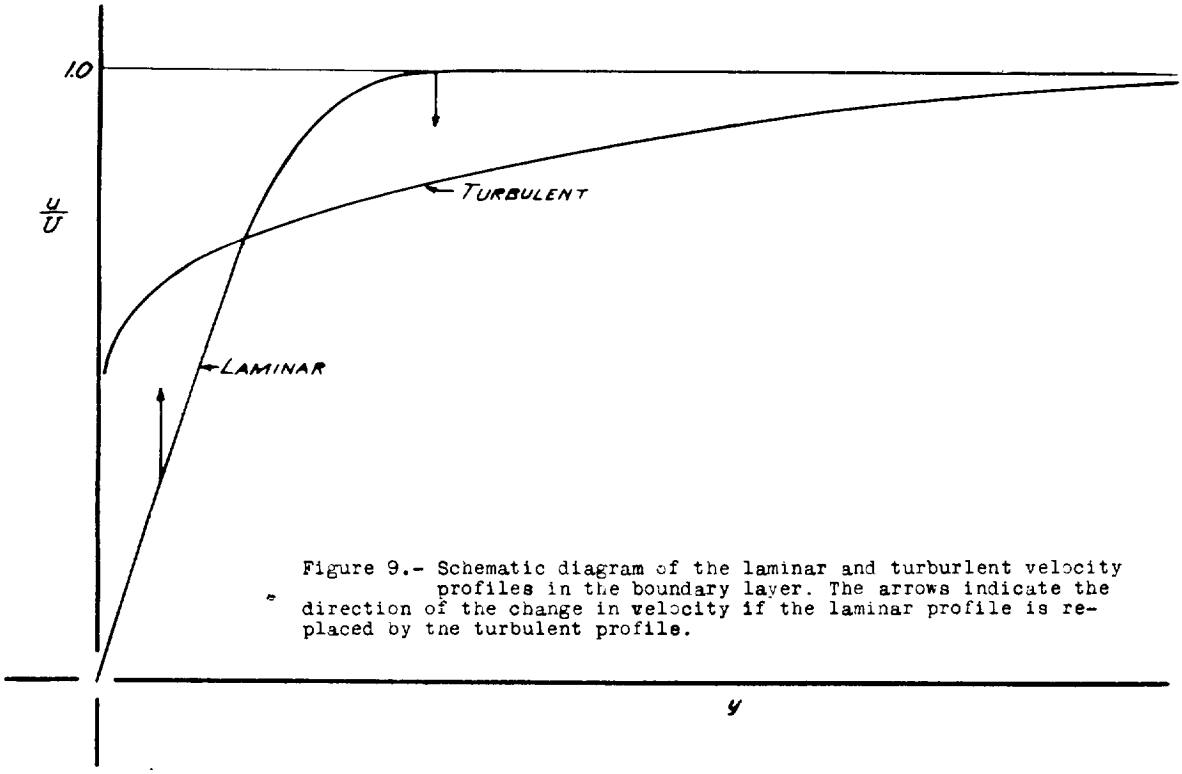

Figure 9.- Schematic diagram of the laminar and turburlent velocity profiles in the boundary layer. The arrows indicate the direction of the change in velocity if the laminar profile is replaced by the turbulent profile.

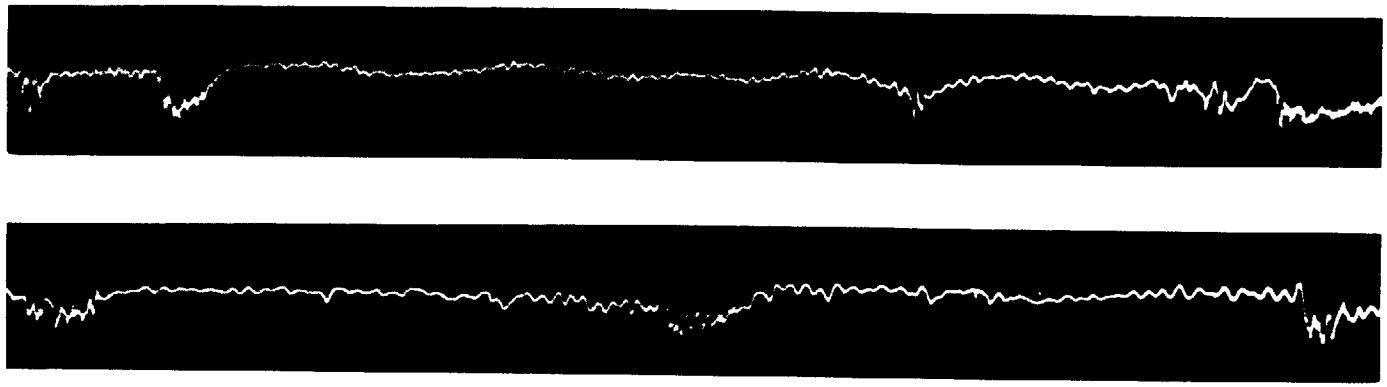

Figure 10.- Oscillograms of velocity fluctuations in the transition region with turbulent "bursts".

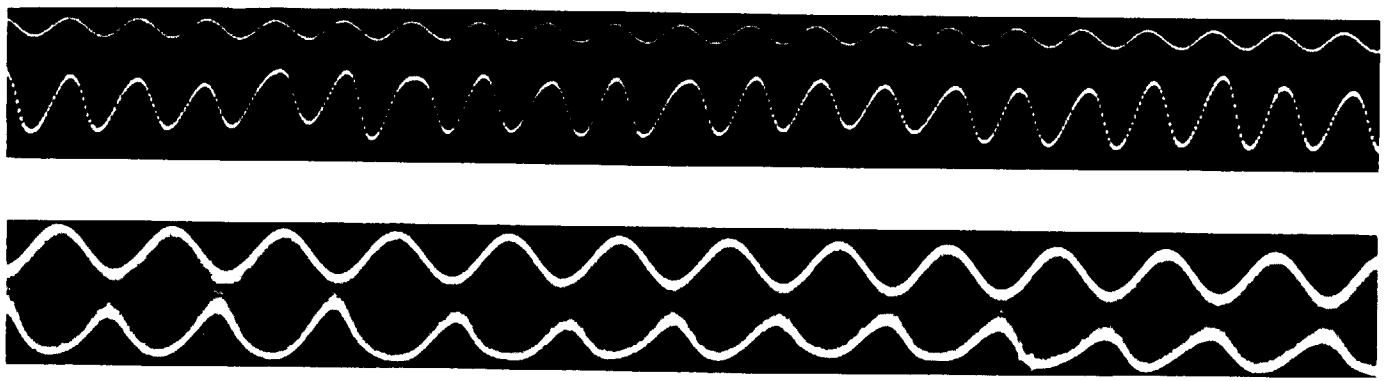

Figure 16.- Regular boundary layer oscillations excited by the wire lattice. The upper trace is the timing wave tuned to the hot wire output (lower trace).

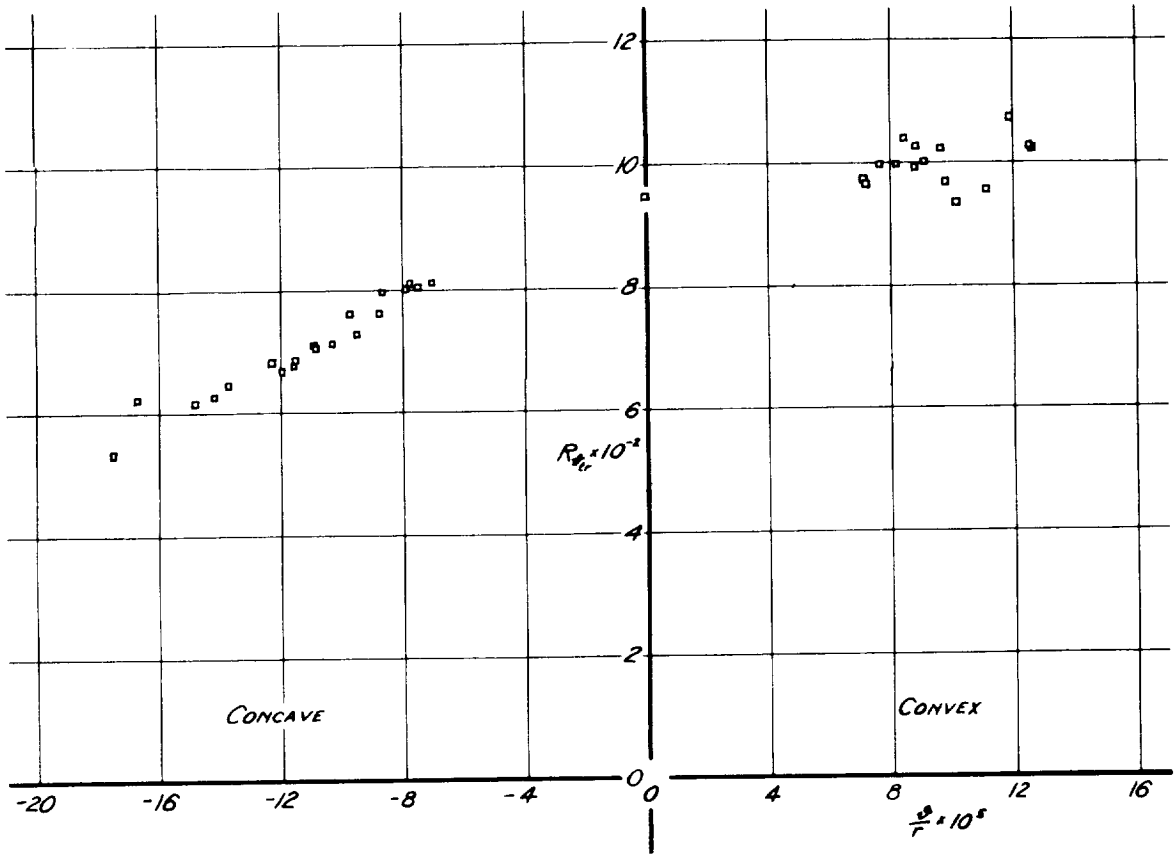

Figure 11.- Effect of curvature on the Reynolds number of transition. Results of measurements on the flat plate and r = 20' plate are shown.

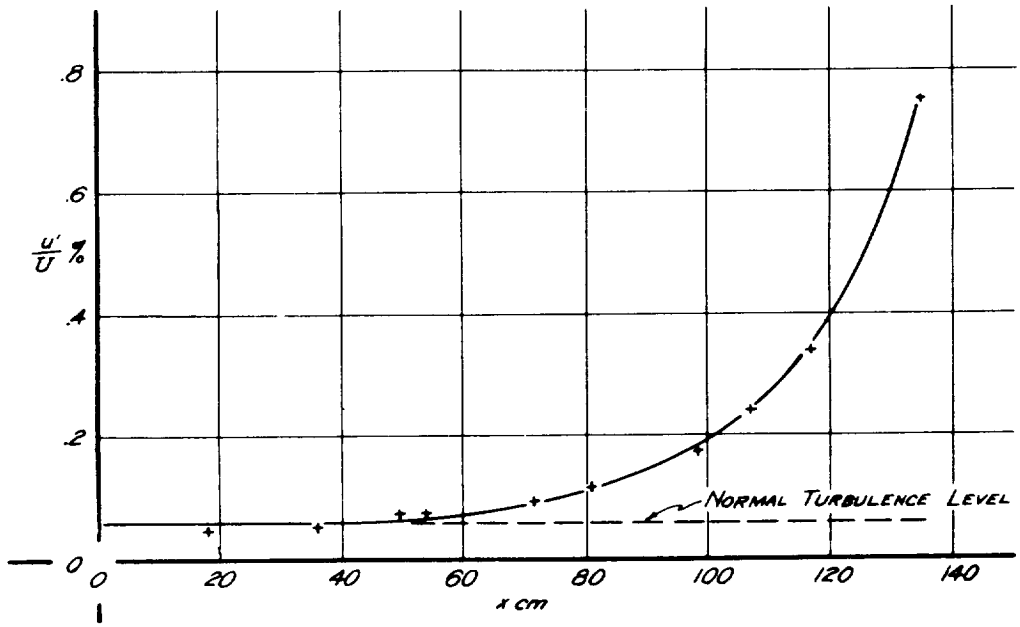

Figure 12.- Increase of turbulence level along convex side of r = 30" plate due to the spread of turbulence from the opposite wall.

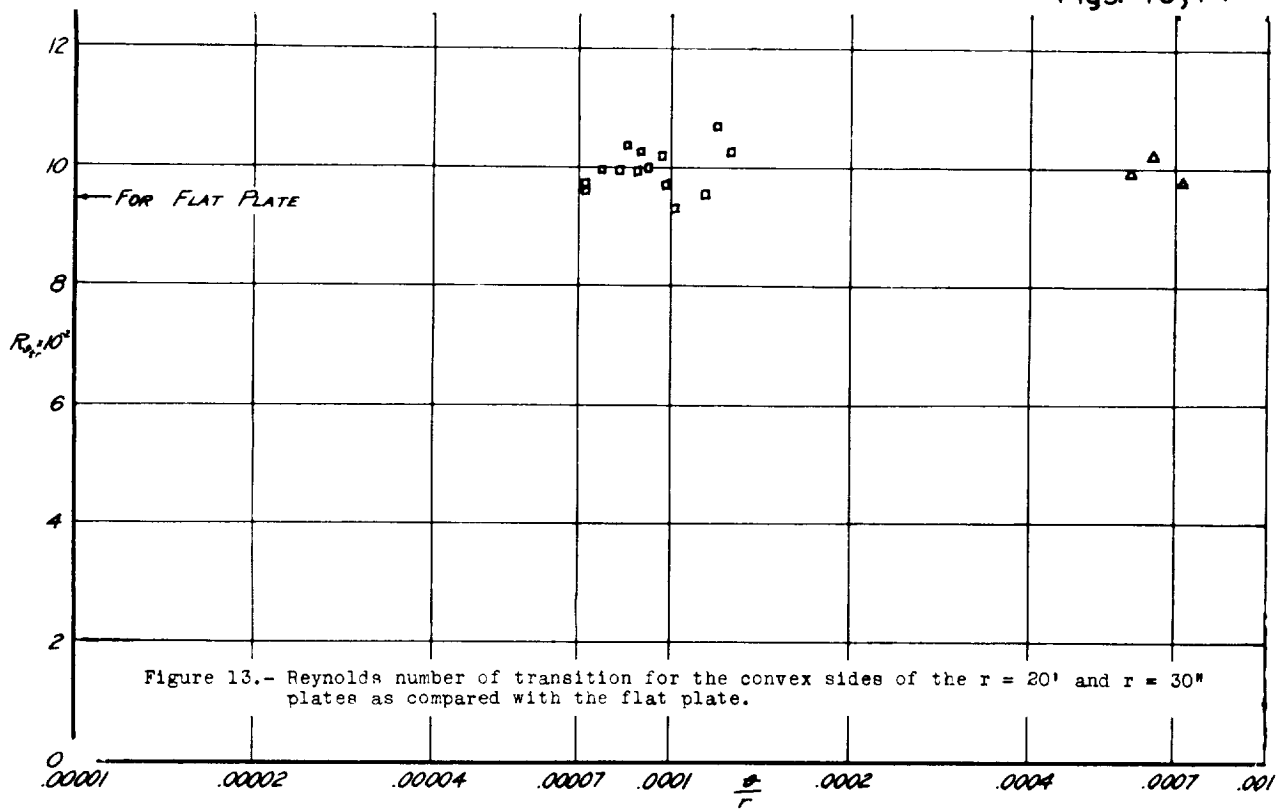

Figure 13.- Reynolds number of transition for the convex sides of the r = 20' and r = 30" plates as compared with the flat plate.

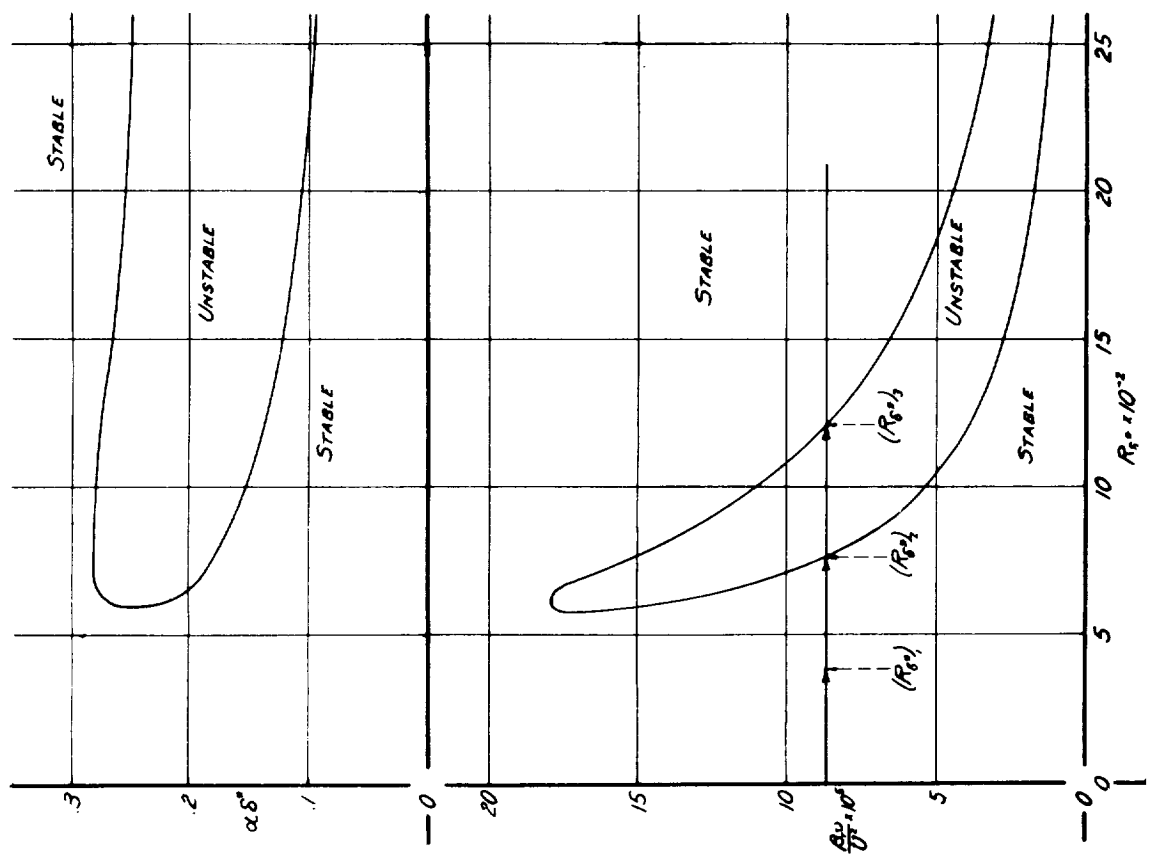

Figure 14.- Theoretical instability limit of the flat-plate boundary layer according to Schlichting.

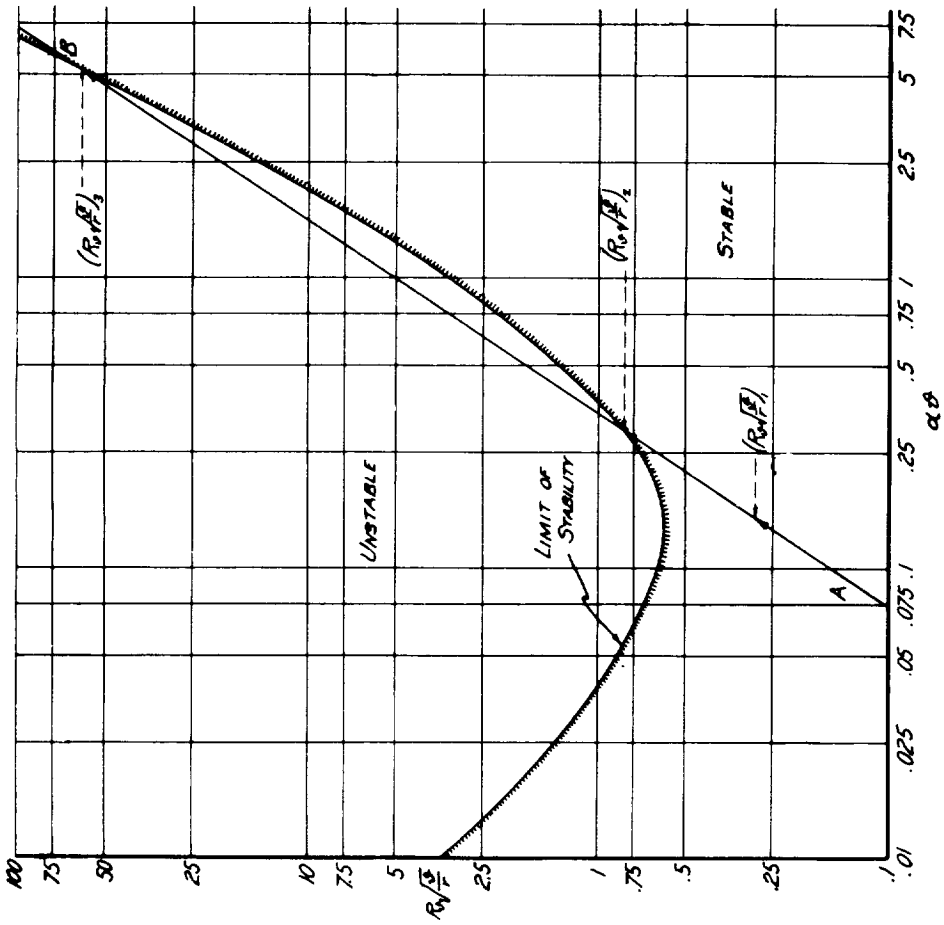

Figure 15.- Theoretical instability limit for the Blasius boundary layer along a concave wall according to Görtler.

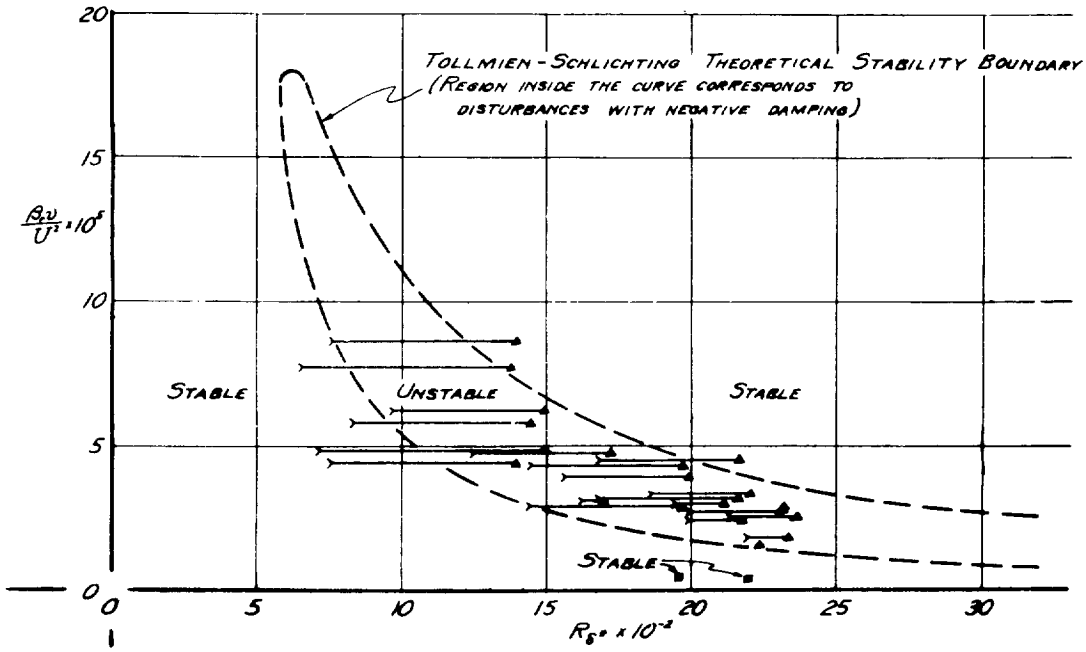

Figure 17.- Frequencies of the boundary layer oscillations excited by the wire lattice as compared with the theoretical instability limit. The horizontal lines denote the path of the amplified waves from the lattice to the beginning of transition.

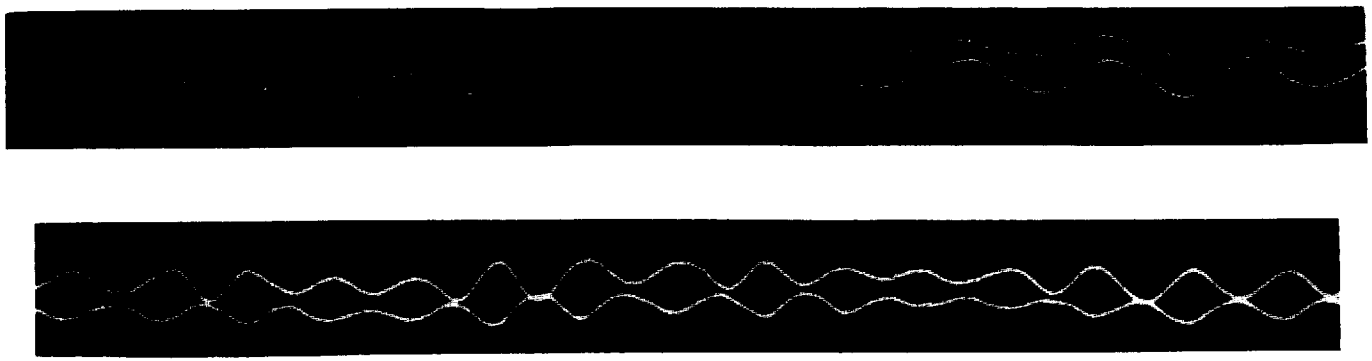

Figure 18.- Correlation between the output of two hot wires in the boundary layer showing the effect of wavelength, wave excited by the wire lattice. Upper trace, $\Delta x/\lambda = 1$; lower trace, $\Delta x/\lambda = 1/2$.

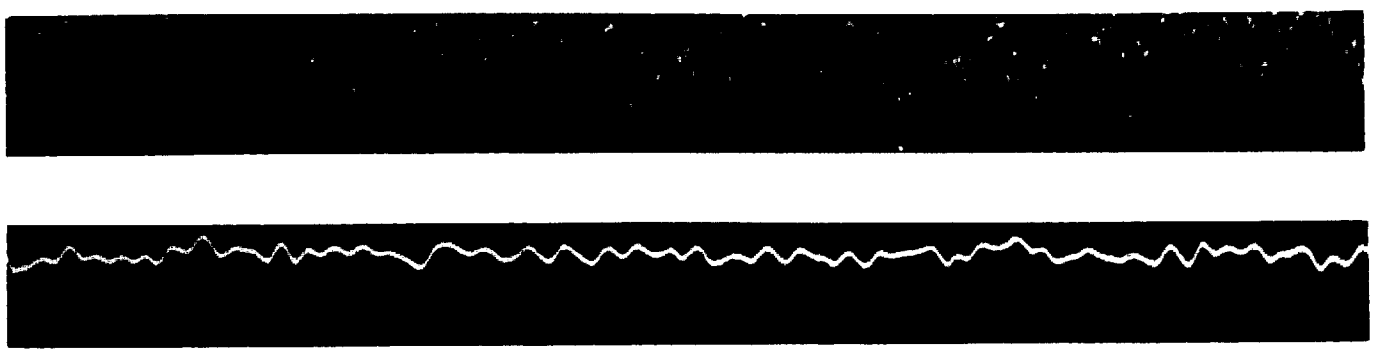

Figure 30.- Velocity fluctuations in the wake of a single roughness element showing the effect of sound waves on the flow in the wake. Lower trace without sound, upper trace with sound. (Compare with fig. 29).

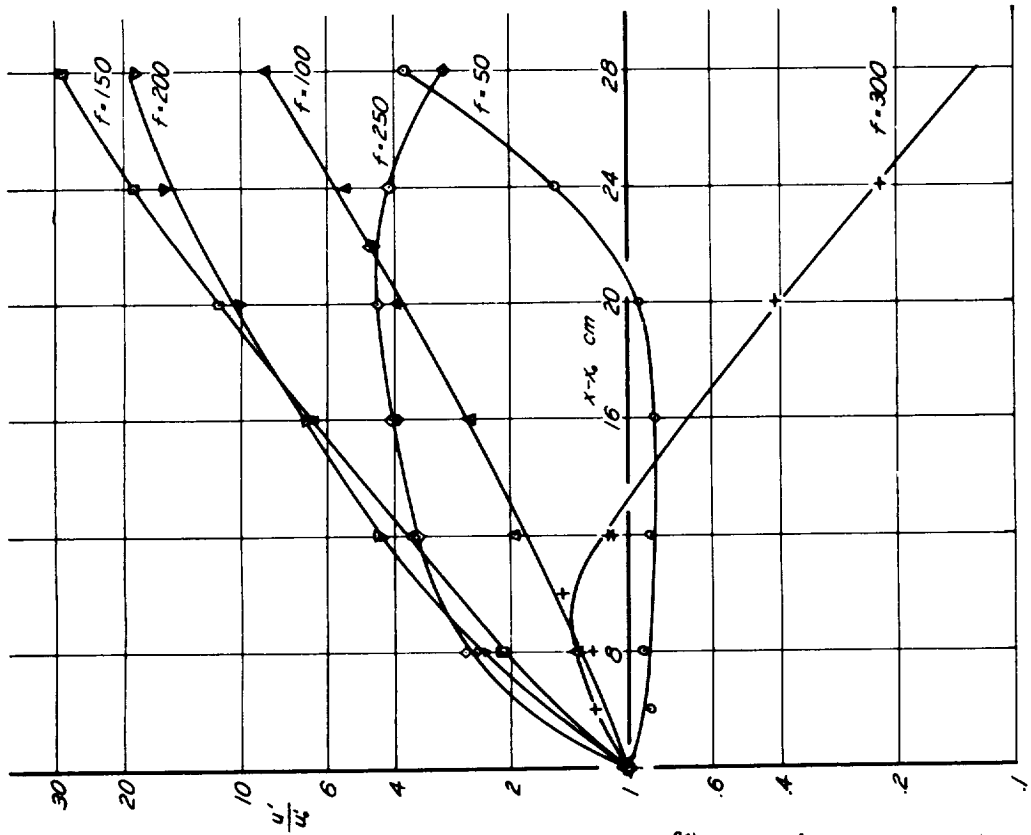

Figure 19.- Relative amplitude of the laminar boundary layer oscillations as function of the distance from the vibrating ribbon. u'_0 denotes the amplitude at a distance of 4 cm downstream from the ribbon.

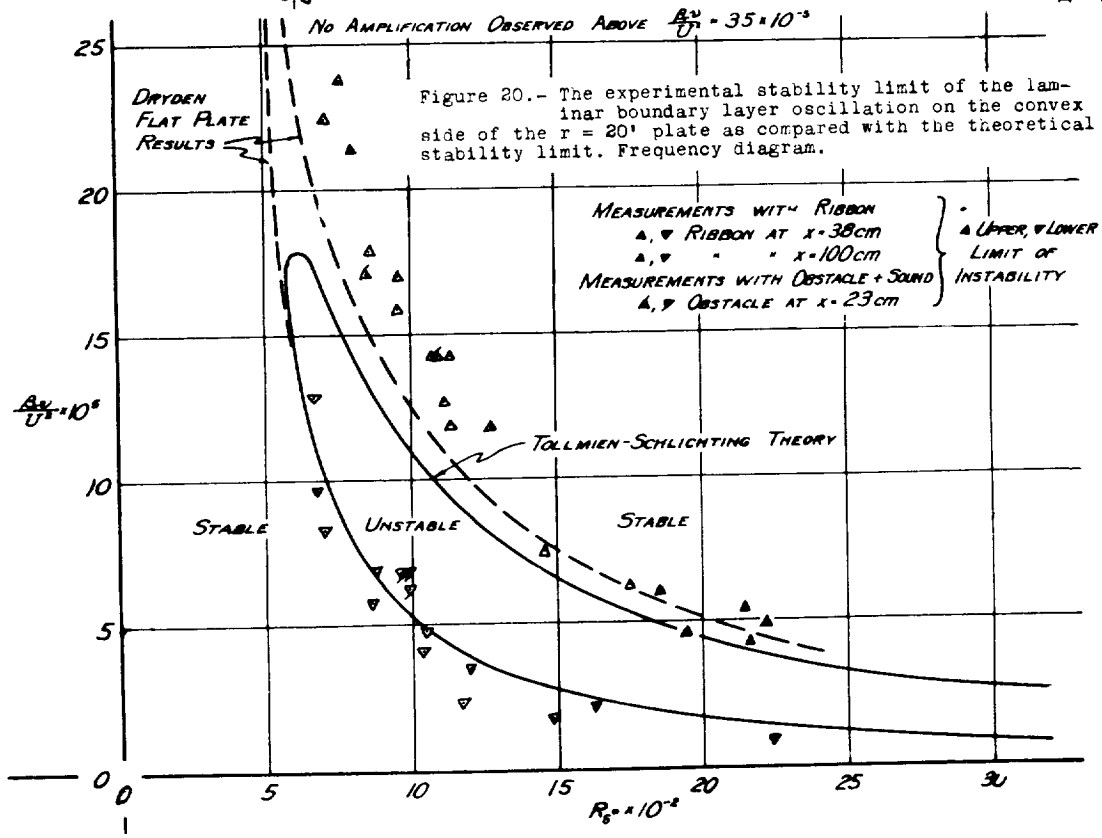

Figure 20.- The experimental stability limit of the laminar boundary layer oscillation on the convex side of the r = 20' plate as compared with the theoretical stability limit. Frequency diagram.

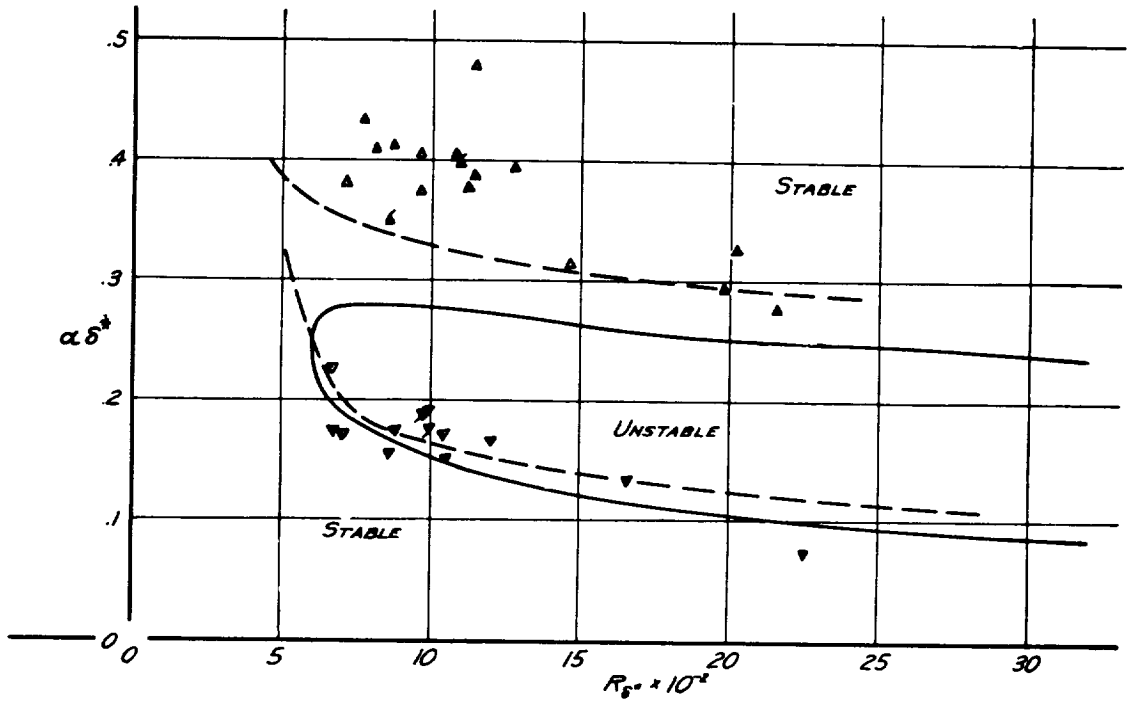

Figure 21.- The experimental stability limit of the laminar boundary layer oscillation on the convex side of the r = 20' plate as compared with the theoretical stability limit. Wave length diagram.

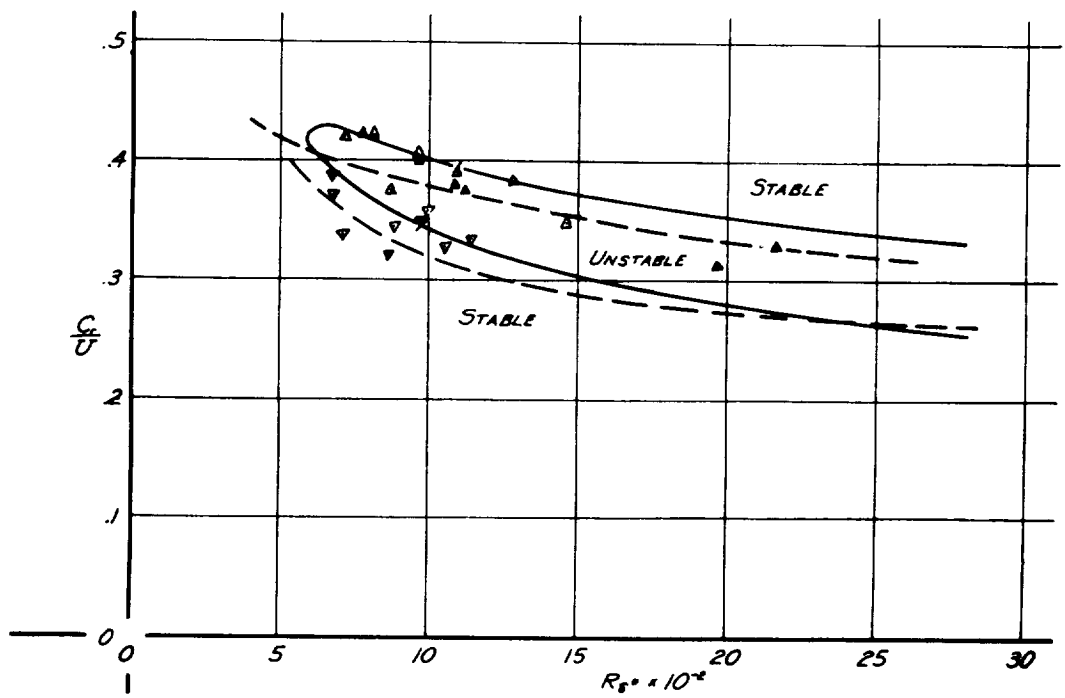

Figure 22.- The experimental stability limit of the laminar boundary layer oscillation on the convex side of the r = 20' plate as compared with the theoretical stability limit. Phase velocity diagram.

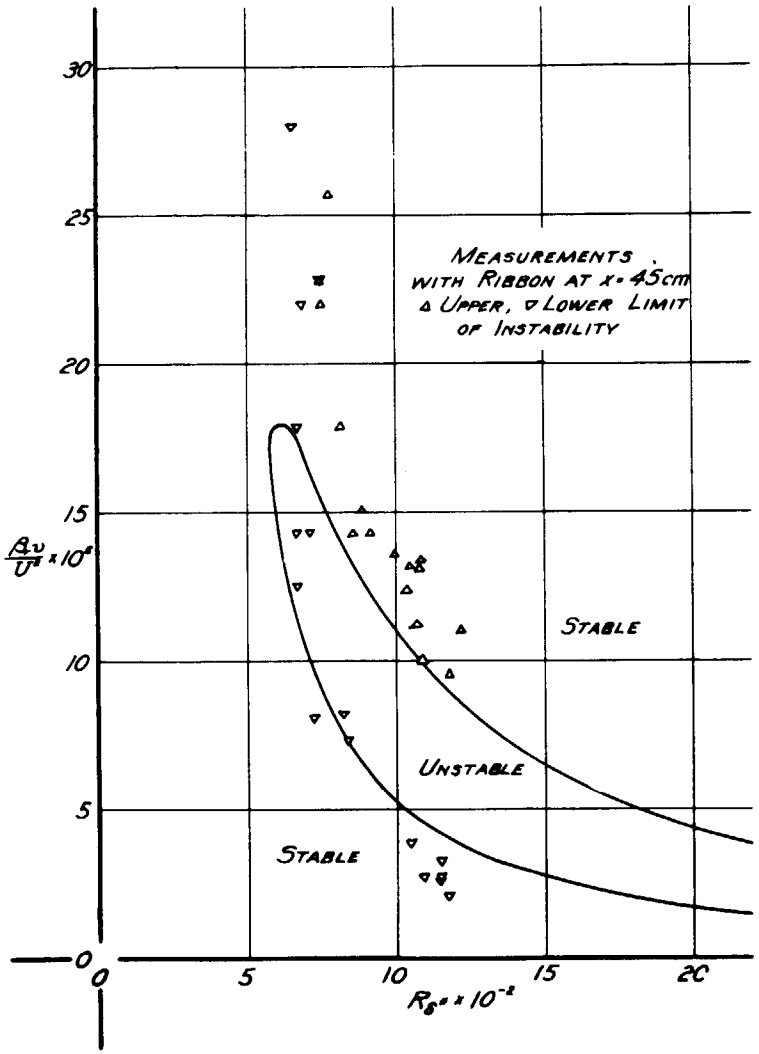

Figure 23.- The experimental stability limit of the laminar boundary layer oscillation on the convex side of the r = 30" plate as compared with the theoretical stability limit. Frequency diagram.

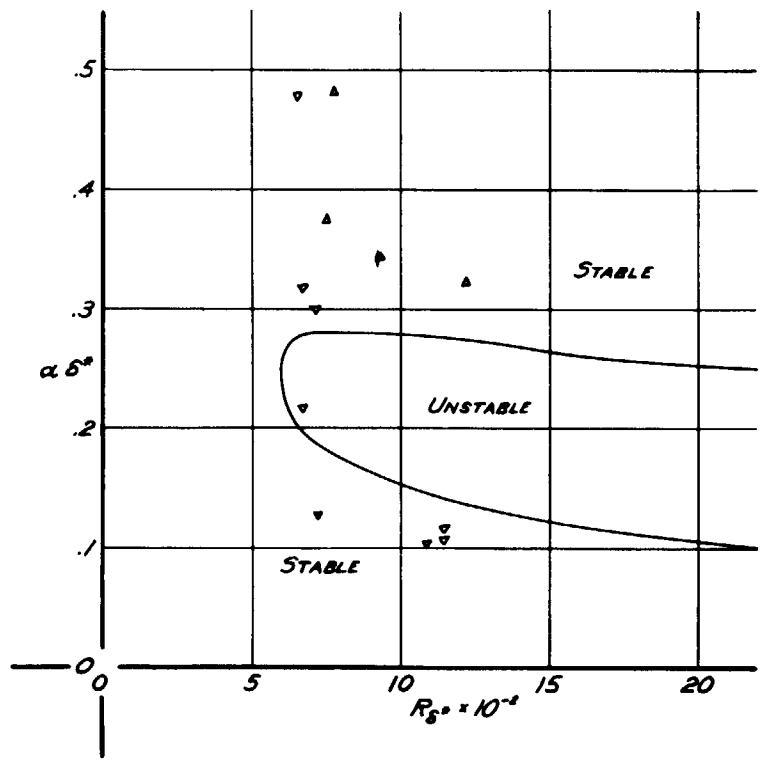

Figure 24.- The experimental stability limit of the laminar boundary layer oscillation on the convex side of the r = 30" plate as compared with the theoretical stability limit. Wavelength diagram.

W-107

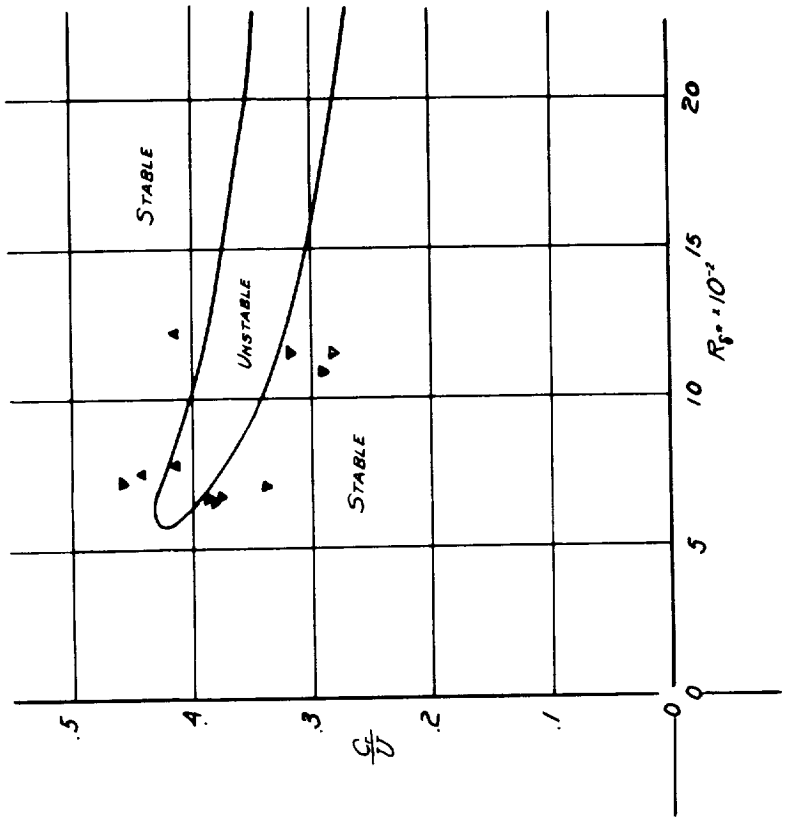

Figure 25.- The experimental stability limit of the laminar boundary layer oscillation on the convex side of the r = 30" plate as compared with the theoretical stability limit. Phase velocity diagram.

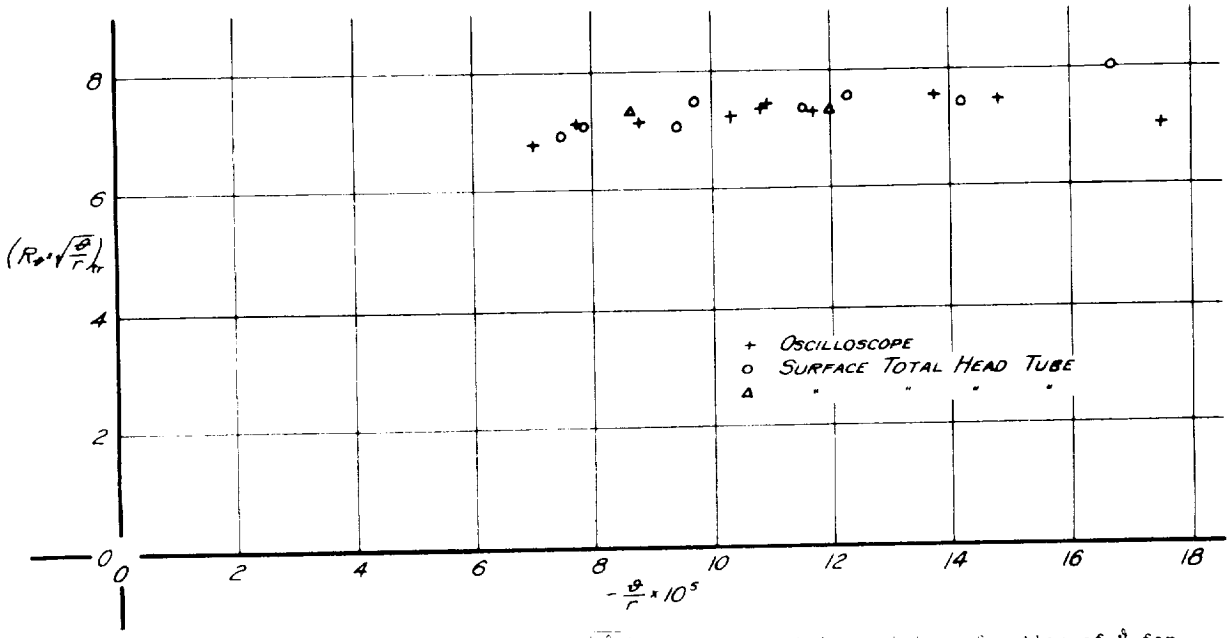

Figure 26.- The critical parameter $\left(R_\vartheta \sqrt{\frac{\vartheta}{r}}\right)$ at the transition point as function of $\frac{\vartheta}{r}$ for the concave side of the r = 20' plate.

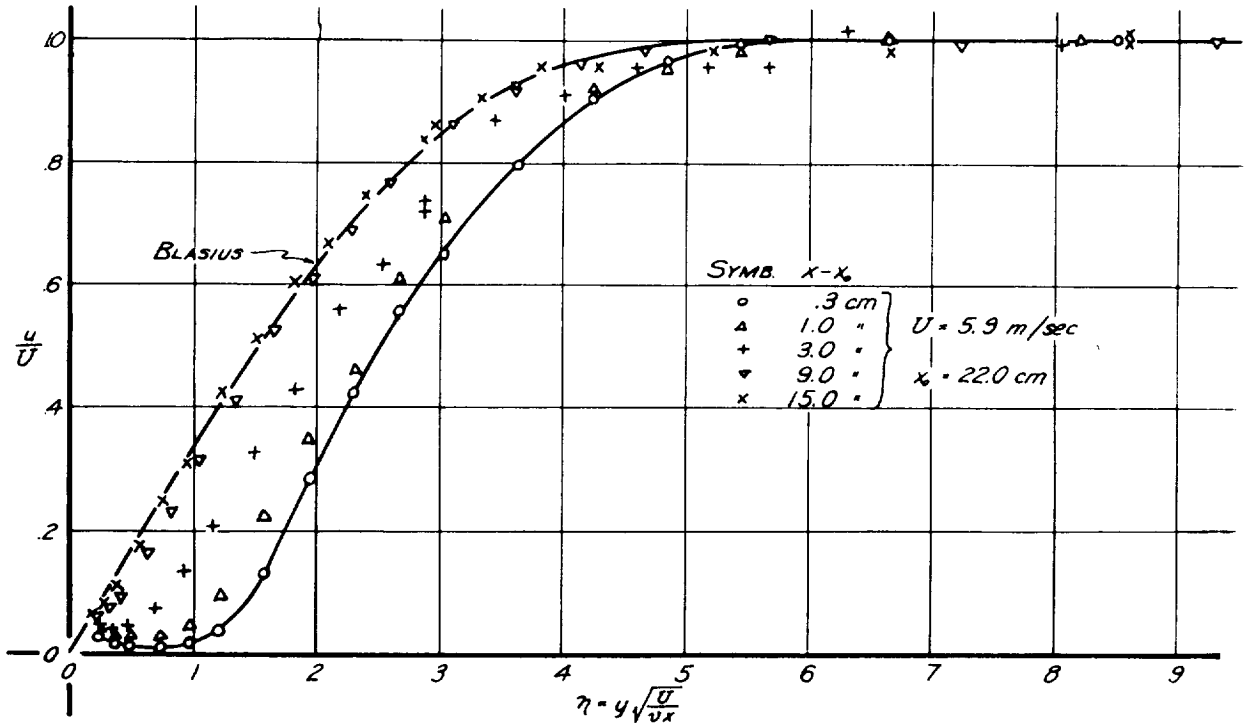

Figure 27.- Velocity profiles downstream from a single roughness element situated at a distance x_0 from the leading edge. The boundary layer returns to the Blasius type profile.

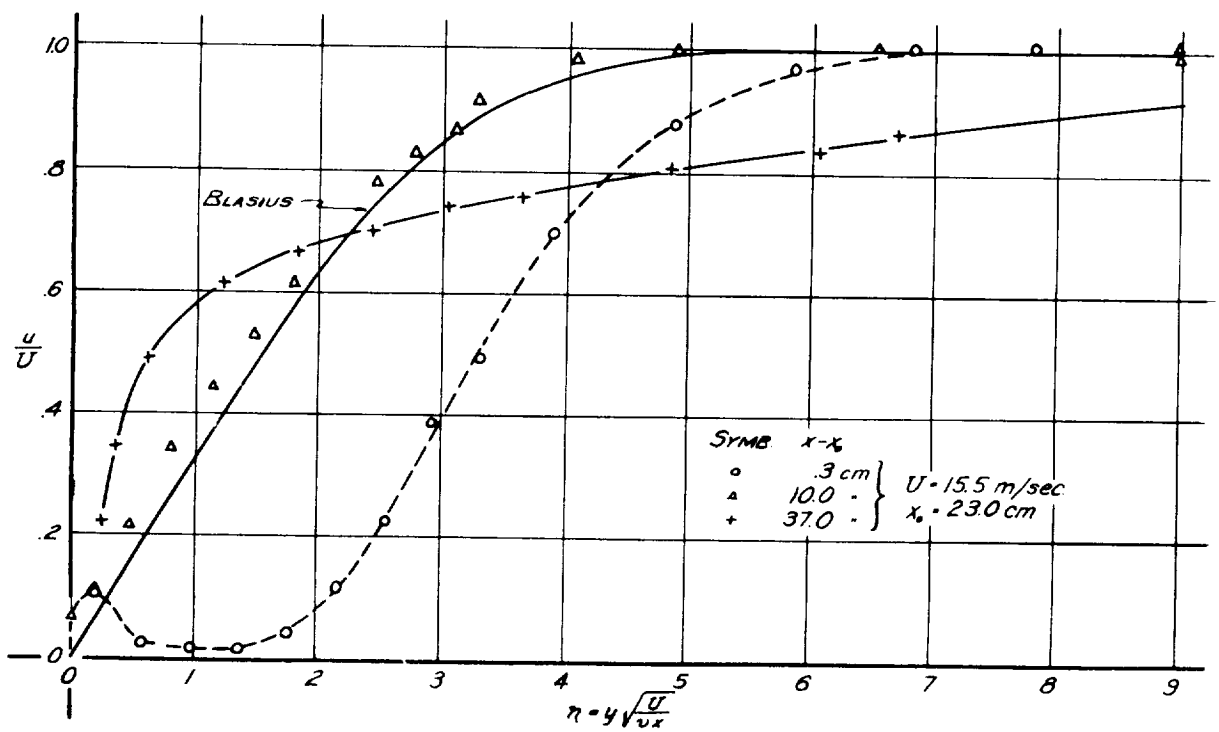

Figure 28.- Velocity profiles downstream from a single roughness element situated at a distance x_0 from the leading edge. Transition occurs after the boundary layer has become reattached to the wall.

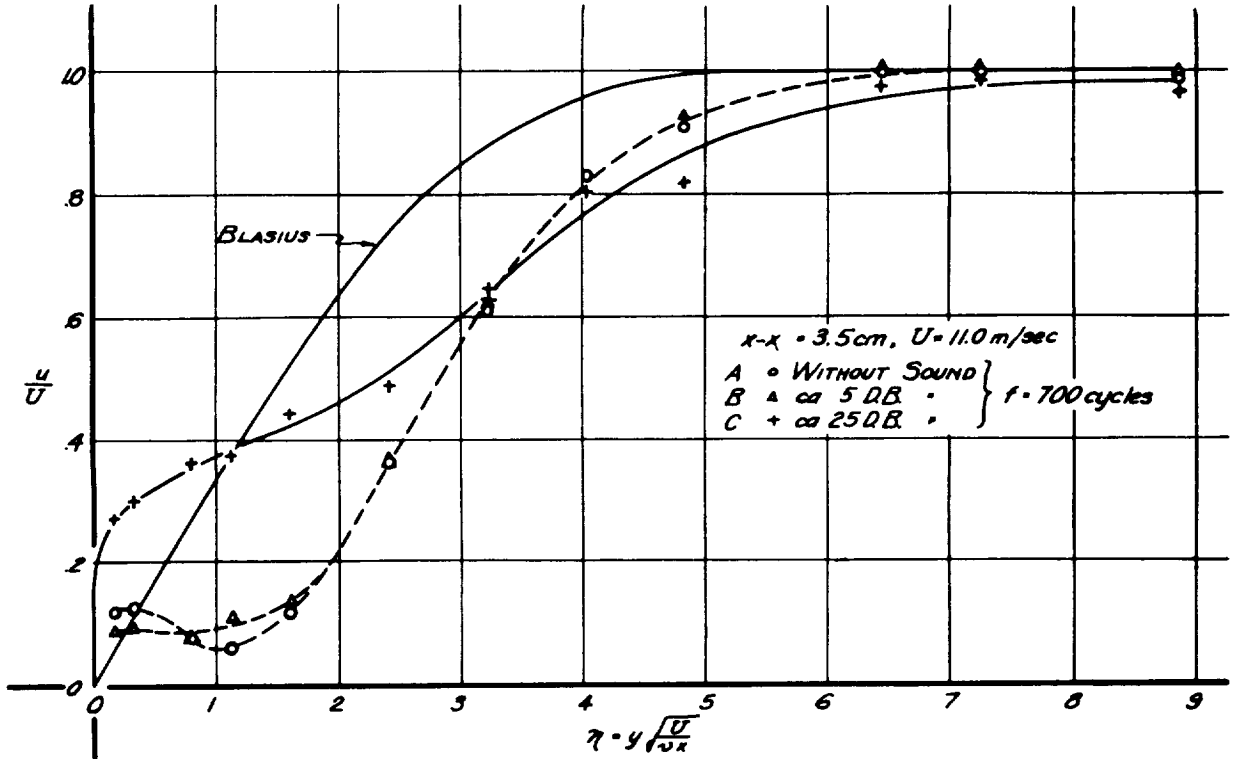

Figure 29.- Velocity profiles downstream from a single roughness element situated at a distance x_0 from the leading edge. The disturbance due to sound waves leads to transition in the wake of the element.

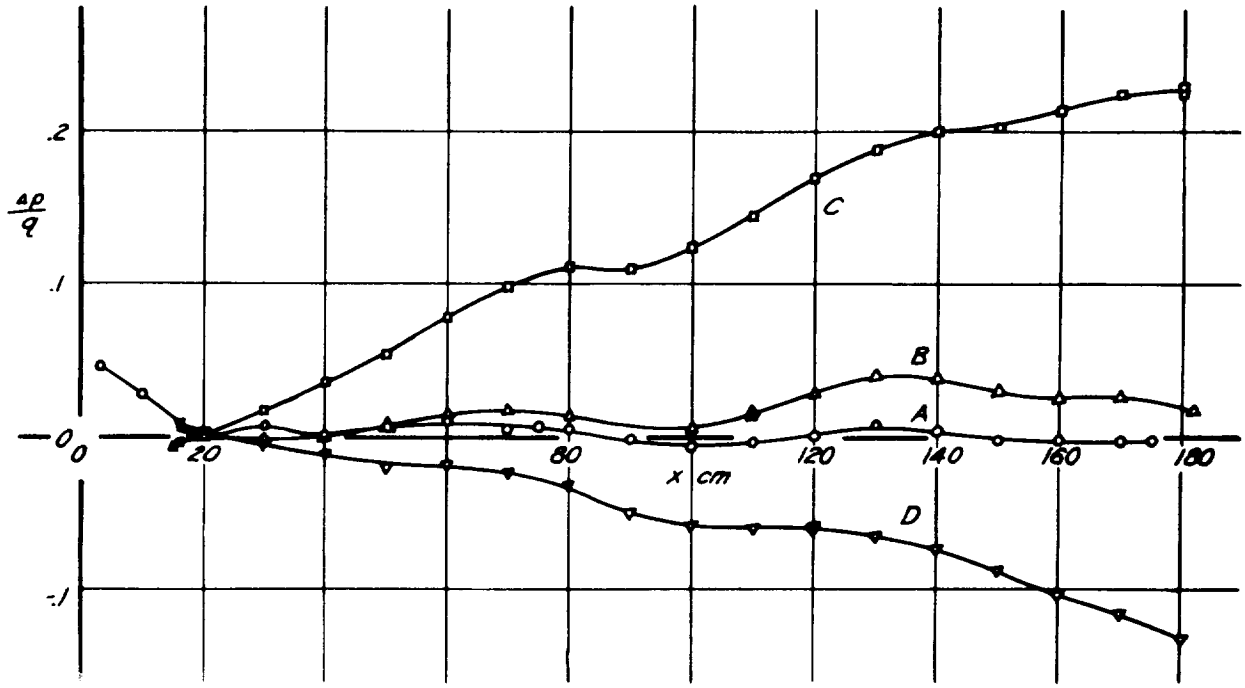

Figure 31.- Pressure gradients for which transition was investigated along the convex side of the r = 20' plate.

W-107

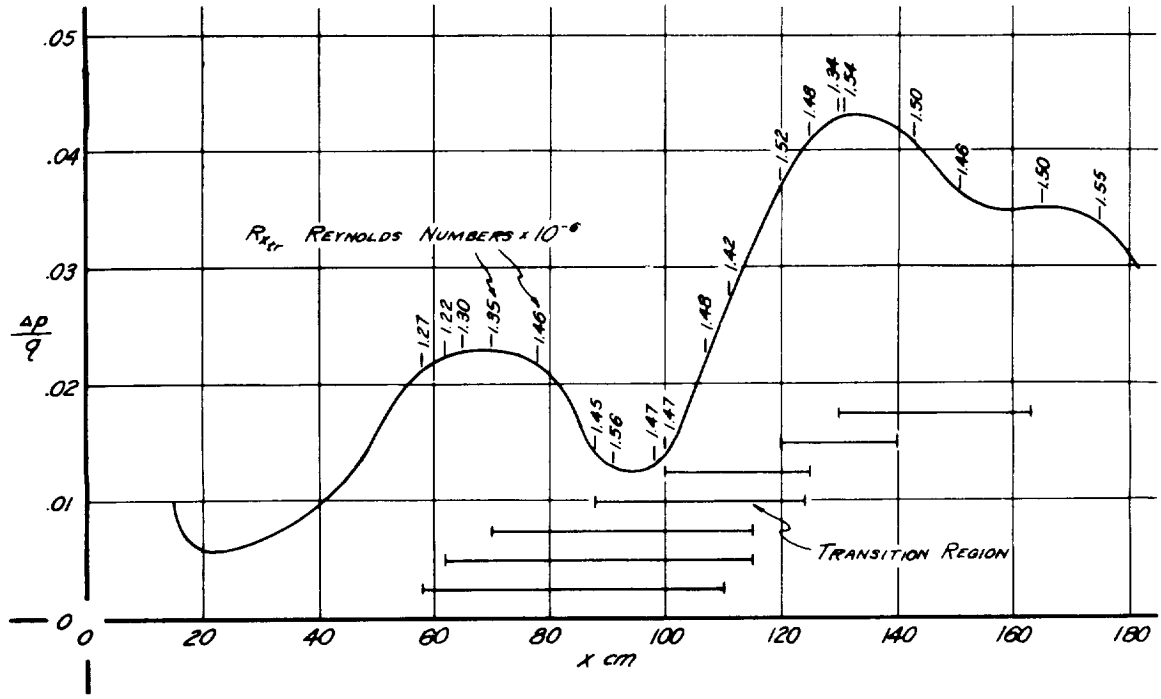

Figure 32.- Reynolds numbers of transition with pressure gradient B. Note change in scale as compared with Fig. 31.

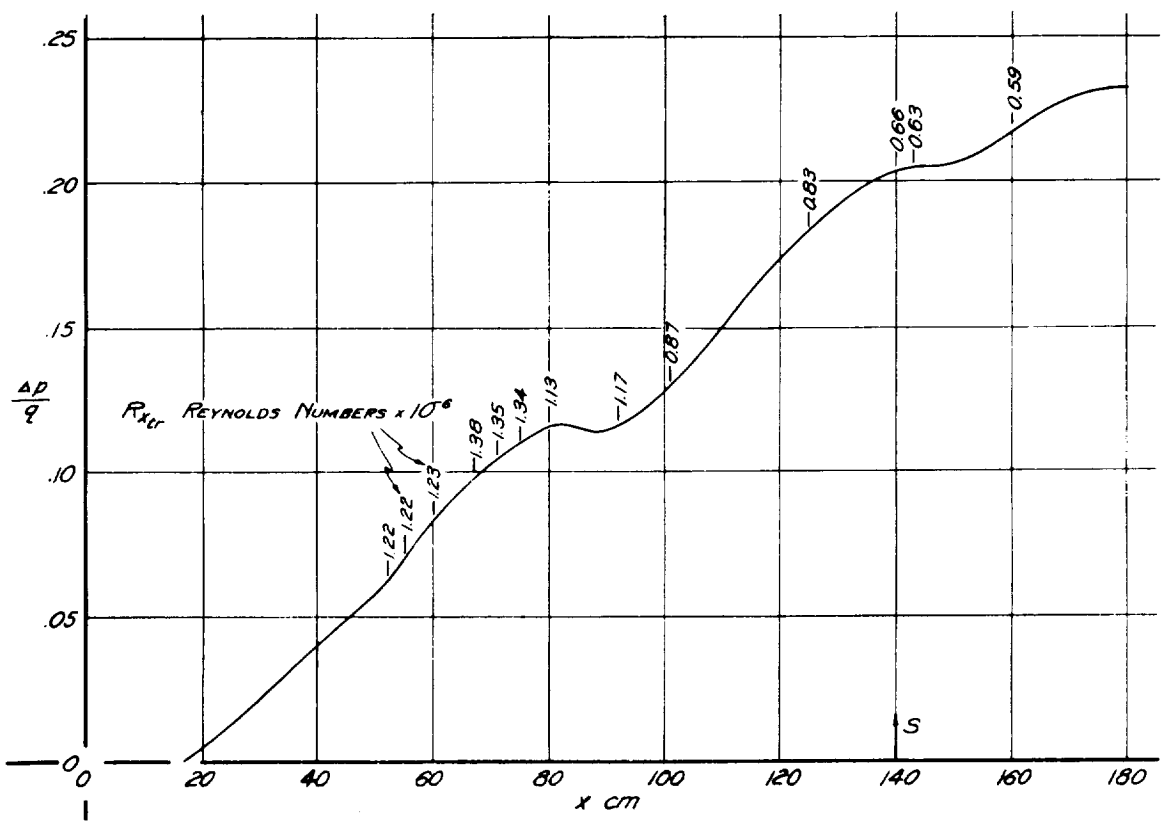

Figure 33.- Reynolds number of transition with pressure gradient C. Note change in scale as compared with Fig. 31. S denoted the computed sepatation point.

W-107

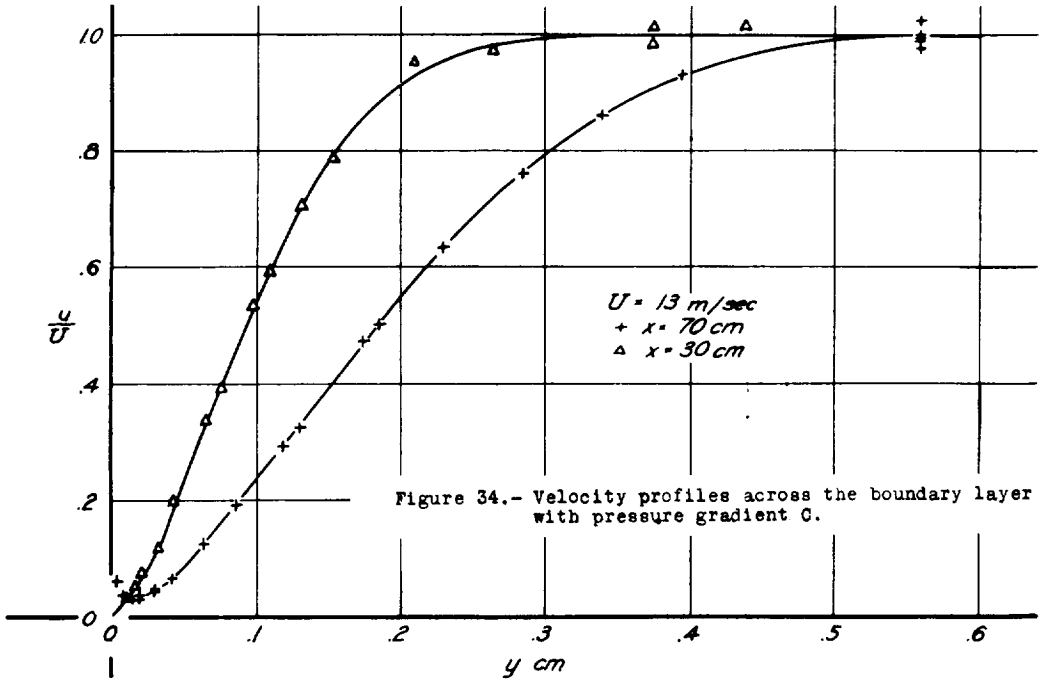

Figure 34.- Velocity profiles across the boundary layer with pressure gradient C.

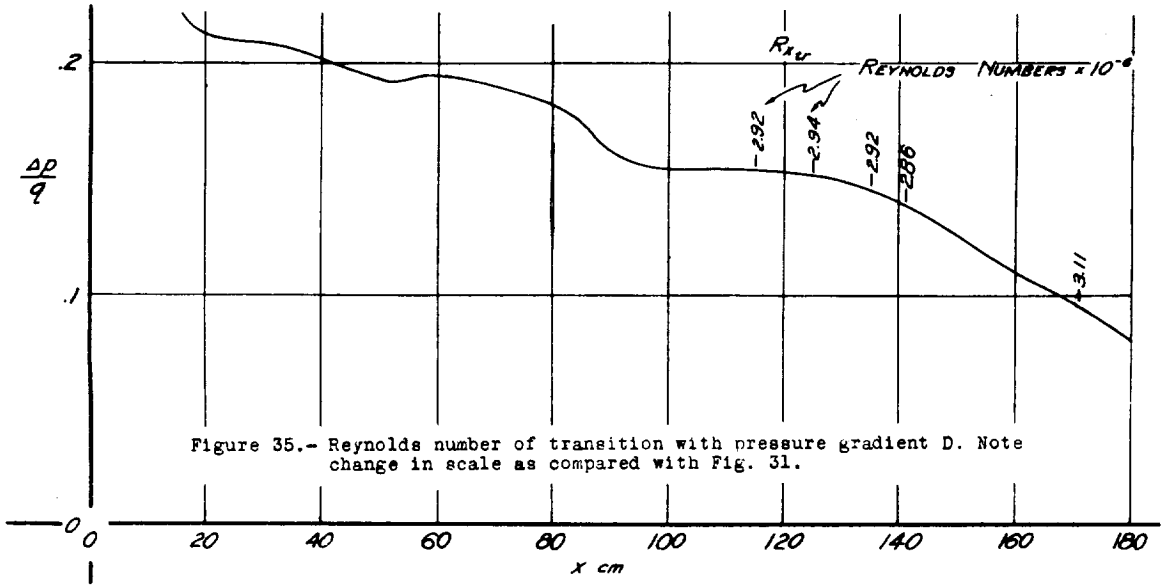

Figure 35.- Reynolds number of transition with pressure gradient D. Note change in scale as compared with Fig. 31.

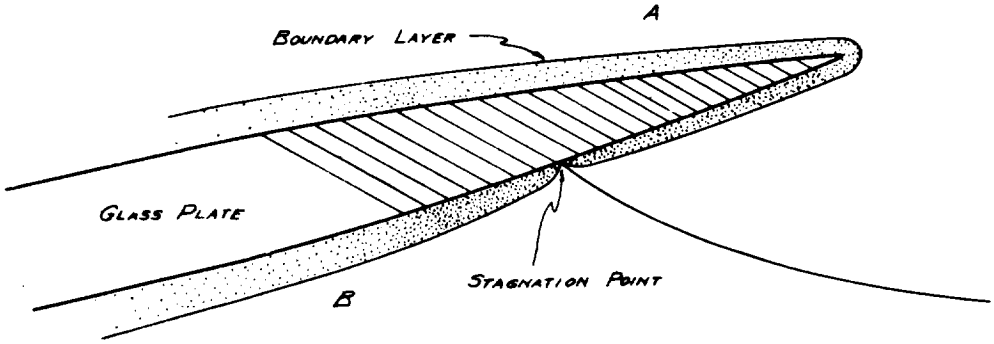

Figure 36.- Schematic diagram showing the angle of attack effect.